ARMY RESEARCH LABORATORY

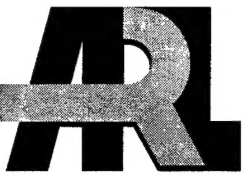

A High Intensity Infrasonic Acoustic Test System

H. Edwin Boesch, Jr., Christian G. Reiff, and Bruce T. Benwell

ARL-TR-2349 November 2001

The findings in this report are not to be construed as an official Department of the Army position unless so designated by other authorized documents.

Citation of manufacturer's or trade names does not constitute an official endorsement or approval of the use thereof.

Destroy this report when it is no longer needed. Do not return it to the originator.

Army Research Laboratory

Adelphi, MD 20783-1197

ARL-TR-2349 **November 2001**

A High Intensity Infrasonic Acoustic Test System

H. Edwin Jr. Boesch

Sensors and Electron Devices Directorate, ARL

Christian G. Reiff

Sensors and Electron Devices Directorate, ARL

Bruce T. Benwell

Directed Energy Technologies

Sponsored by

TACOM/ARDEC

Picatinny Arsenal NJ 07806

Abstract

We describe the design, mathematical modeling, construction, and test of an acoustic test system intended to support the performance of high-intensity acoustic effects experiments on large targets at low-sonic to infrasonic frequencies. An early experimental version of the system, HILF1, used a compressed-air source and airflow modulator from the ARL Mobile Acoustic Source (MOAS) and a single-volume Helmholtz resonator test chamber to achieve sound pressure levels (SPL) above 140 dB in a 5-m^3 volume. Based on results from this system, a more advanced system, HILF2, was designed and built. HILF2 uses a compressed-air source based on automotive superchargers, a low-impedance airflow modulator, and a two-volume Helmholtz resonator test chamber to achieve sustained high-purity sinusoidal sound pressure levels in excess of 155 dB in a 2.5-m^3 test volume at frequencies from 2 to 20 Hz.

Contents

Figures

Tables

1. Background

For several years, the Department of Defense Joint Non-lethal Weapons Directorate (JNLWD), through the Close Combat Armaments Center (CCAC) at the Tank-Automotive and Armaments Command/Armament Research, Development and Engineering Center (TACOM/ARDEC), sponsored an effort to demonstrate acoustic technologies that may be useful for nonlethal weapons. The U.S. Army Research Laboratory (ARL) has supported this effort with field and laboratory measurements and research on the design of high-intensity acoustic sources. These sources include both potential acoustic weapons and laboratory sources for use in exploring the effects produced on targets by high-intensity sound.

In May 1998, in support of the effort by the JNLWD to assess the effectiveness of high-intensity sound as an acoustic weapon, we addressed the problem of designing a test facility for low-frequency acoustic effects experiments [1]. Of particular interest was continuous (nonimpulsive) sound in the high-infrasonic frequency range from a few Hertz to just below human audibility (below about 20 Hz) and sound pressure levels (SPL) in the range from 140 to 160 dB (referenced to 2×10^{-5} Pa). A long history of anecdotal and some direct referential evidence has suggested that sound in this range may be capable of affecting human behavior through discomfort, disorientation, or distraction without producing permanent physical damage. However, few laboratory facilities were available to the DoD for investigating the effects of sound in this frequency and intensity regime. The purpose of this effort was to design a high intensity infrasonic source that would support such bio-behavioral effects experiments. *In particular, the original goals as set forth in [1] were to design and construct a test facility that would (1) provide a test volume sufficient to hold moderately large test items or subjects (about 2 to 5 m^3), operate over a frequency range from about 20 Hz down to about 5 Hz, and (3) provide a uniform sound field in the test volume with an accurately controllable SPL up to 160 dB.*

The generation and radiation of controllable, intense, continuous sound at low audible and infrasonic frequencies—below 30 Hz—into open air is a difficult task. The dimensions of practical sources are much smaller than the large wavelengths involved (e.g., nearly 60 ft at 20 Hz) and therefore are inefficient at coupling acoustic energy into free space. As a point of reference, the bulk of the cost of a high-quality home or theater loudspeaker system is associated with the reproduction of the low audible frequencies from above 20 Hz to several hundred Hz at intensities well below 120 dB—power densities thousands of times lower than our goal.

Figure 1 shows the high infrasonic acoustic regime with respect to the audible frequency range. Also shown are the approximate frequency ranges

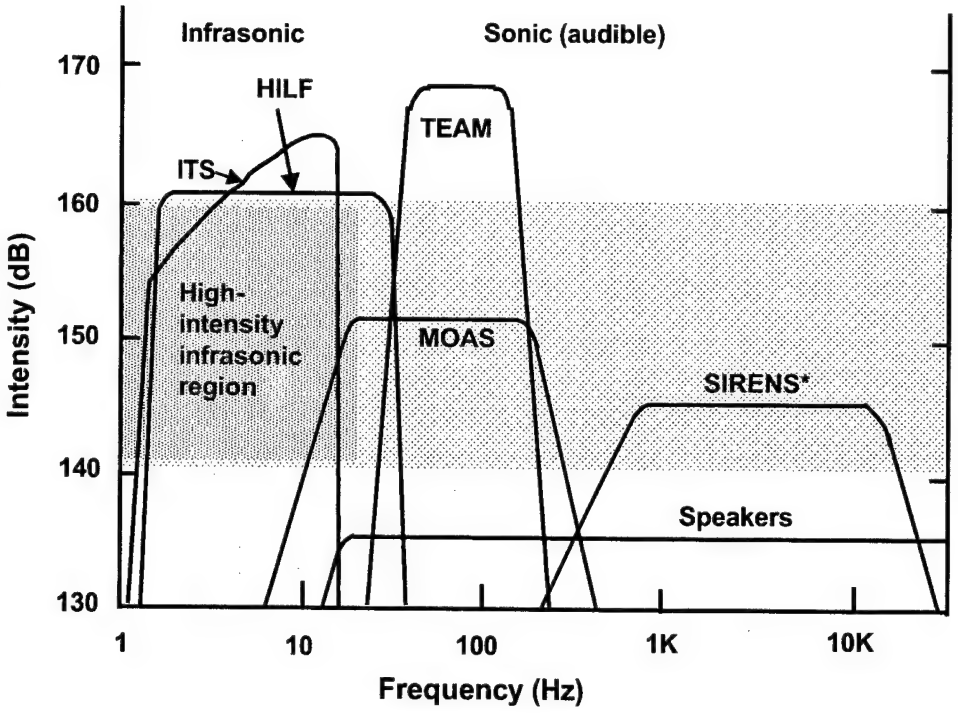

Figure 1. Ranges of frequencies and sound intensities produced by certain sound sources and acoustic test facilities.

and intensities attainable with several laboratory and generic continuous wave sound sources. The ARL Mobile Acoustic Source (MOAS) is a large horn driven by a modulated compressed airflow capable of continuously producing SPLs up to 155 dB at frequencies from 20 to 300 Hz. The TEAM device operated by the National Testing Service modulates a high-pressure compressed airflow into an open-end test chamber/acoustic transmission line with a servo-driven fast valve. It is capable of very high SPLs (approaching 170 dB) in 30-s bursts over a frequency range from about 40 to 200 Hz. The Infrasonic Test System (ITS) operated by the Air Force Research Laboratory is a small (less than 1 m^3) test chamber in which infrasound is generated by mechanically driving a large piston sealed into one wall of the chamber. This system is capable of SPLs above 160 dB at its upper frequency limit (about 20 Hz). The ITS was the only source capable of covering the infrasonic frequency and intensity region of interest; unfortunately, its small size limited its use to small animals or test objects. In addition, since the sound intensity varied with frequency and the sound intensity could not be varied, it was impossible to identify intensity and frequency effects thresholds.

2. Introduction

In a previous report [1], we described the design, construction, and performance characterization of a first-generation experimental acoustic chamber. This system, called HILF1 (high-intensity, low-frequency no. 1), was the test vehicle for our first design for a system intended to support acoustic effects studies at high intensities in the high-infrasonic frequency range. Our design took advantage of the high gain present within a Helmholtz resonator, yet it has the frequency tunability of a ported bass reflex enclosure (a Helmholtz/bass reflex hybrid of sorts). Our design consisted of a structurally massive sealed chamber of moderate volume with a port vented to free space (atmosphere). The chamber was driven by modulating a dc flow of air. By varying the port length, we could tune the source to be resonant over the frequency band of interest. At resonance, the maximum sound intensity would be achieved since the equivalent impedance of the source would be entirely real (resistive) with no energy being stored in the reactive portion of the acoustic impedance.

HILF1 successfully proved our design principles and produced continuous SPLs in excess of 140 dB over a frequency range of 5 to 20 Hz within a test volume of moderate size (5 m^3). However, as we shall discuss below, HILF1 was a proof-of-principle experiment and not a usable test system. Further, in the course of measuring the performance of HILF1, we identified major design changes that would lead to a follow-on system with improved performance and usefulness for effects studies.

We first review briefly the basic principles and issues associated with the design of HILF1. We then discuss the shortcomings identified with HILF1 and our proposed solutions. Next follows a discussion of the theory and design of our new system—HILF2—and modeling of the expected performance of this system. Finally, we report the results of measurements of the performance of HILF2 operated in three different configurations and at different frequencies.

3. Design Concept for the Infrasonic Test Chambers

The goals for the second-generation infrasonic source (HILF2) were (1) a test volume sufficient to hold test items and associated experimental apparatus (2 to 5 m^3), (2) a frequency range capability from about 5 to 20 Hz, and (3) a uniform sound field in the test volume with an accurately controllable intensity up to 160 dB.

Both HILF1 and HILF2 consist of a closed chamber driven by acoustic energy from a flow modulator and a compressed air source. (A flow modulator is essentially a valve that creates acoustic energy from a continuous (dc) airflow by periodically varying that flow.) The use of a closed chamber concentrates the acoustic energy in a small volume, isolates the surroundings from the acoustic energy, and also makes possible the amplification of the acoustic intensity in the chamber by tuning the chamber to resonate at the desired frequency. The HILF chambers are forms of a Helmholtz resonator. A Helmholtz resonator consists of a compressible (closed) air volume (acoustic compliance) connected to a duct or port with a freely moveable air mass (acoustic mass). The two resonate at a characteristic frequency in the manner of a mass attached to a spring. Helmholtz resonators (one form is familiar to audiophiles as the bass reflex loudspeaker enclosure) operate at wavelengths greater than their largest dimensions and consequently produce nearly uniform sound fields throughout their volumes.

A major portion of the phase I effort included developing a theoretical model to aid in designing the infrasonic source as well as complementing/validating the experimental work. Fortunately the complex task of developing a theoretical model could be simplified by taking advantage of the fact that the wavelength of the sound field would be much larger than the largest dimension of the infrasonic chamber. This allowed us to represent the acoustic elements using lumped parameters. The model we developed translates each acoustic element into an equivalent electrical component (i.e, acoustic compliance to capacitance, acoustic mass to inductance, losses to resistance, mass air flow to current, pressure to voltage). The end result was the development of an equivalent circuit electrical model [1].

3.1 Lessons Learned From the HILF1 Modeling and Experiments

The main components of HILF1 were (1) the Helmholtz resonator chamber/test volume, (2) a commercial voice-coil-actuated flow modulator driven by an audio signal generator-amplifier source, and (3) a piston-type air compressor driven by a diesel engine. The modulator and air compressor were parts of the ARL MOAS and were borrowed from the ARL Atmospheric Effects Branch for the HILF1 proof-of-principle tests. Airflow from the compressor and modulator was piped directly into the chamber/resonator. The

chamber was a 5- × 5- × 7-ft concrete-walled water tank (commercial grease trap); its interior was vented to open air with an adjustable port. The chamber/port combination was tuned to the desired frequency by varying the length of this port.

As discussed in [1], we modeled the behavior of the HILF1 system using a lumped-parameter electrical circuit analog with circuit elements calculated from the equivalent acoustic elements of the system. In this model, voltage and current are equivalent to acoustic (ac) pressure and airflow. Acoustic loss elements (e.g., wall absorption, viscous losses in the port, and radiation of acoustic energy from the port) are modeled as resistors. Air-mass inertia or acoustic masses (e.g., port mass) are modeled as inductors, and compressible air volumes or acoustic compliances (e.g., chamber volume) are modeled as capacitance. Expressions for the acoustic elements in terms of the physical properties and dimensions of the various parts of the system were either derived by hand or taken from Beranek [2] or Seto [3] and are listed and discussed briefly in appendix A.

Experimental studies of our infrasonic chamber validated with high accuracy our use of an equivalent circuit electrical model for the chamber response and most of the elements in the model. The models for the reactive elements (acoustic masses and compliances) were found to be particularly accurate since these terms are based on geometrical properties of the system; however, the chamber losses used in our initial calculations included just one poorly understood effect—wall absorption. When the response of the real HILF1 system was measured, the experiments demonstrated that the chamber functioned as expected as a Helmholtz resonator and was driven successfully by the modulator/air compressor at frequencies from 5 to 20 Hz to SPLs in the chamber in excess of 140 dB (20 μPa reference). The measured resonant frequencies for several port configurations matched the model predictions within a few percent. However, the measured SPLs at resonance were roughly 15 dB below the predicted values near 155 dB, and the measured Q of the chamber (the ability of the chamber to store acoustic energy) was substantially lower than the predictions. These results indicated that the acoustic losses in the chamber were larger than expected. Increasing the loss in the model brought the model predictions into reasonable agreement with the measurements. However, we were not able to identify the cause of the additional losses. Reference [1] discusses possible sources of the additional losses and the experimental results from several tests to mitigate these losses. These tests indicated that even if we were able to identify the major sources of acoustic loss in the HILF1 system, from a practical standpoint it is unlikely that we could reduce these losses substantially. Therefore, to increase the SPL in the chamber, we must either increase the source acoustic power, couple or transfer this power into the chamber more effectively, increase the efficiency of the chamber, or all of the above.

3.2 Improvements to the HILF1 Design

At resonance, the infrasonic chamber presents a very low equivalent impedance, approximately 2 kΩ. This is the major reason that it is so difficult to generate intense infrasonic sound intensity and nearly impossible to efficiently match and radiate this energy to free space. The HILF1 model showed that the largest overall SPL increase could be achieved by maximizing the airflow into the chamber while at the same time minimizing the impedance mismatch between the air source and the chamber. These goals formed the basis of the HILF2 design.

3.2.1 DC Air Source

A large increase in the dc air source power is not feasible—an SPL increase of 10 dB by this means would require increasing our compressed airflow by a factor of 10, and the MOAS source already used a 150-hp compressor! We can, however, make a modest increase in the dc source acoustic power and at the same time lower the source impedance (increase airflow for the same pressure). The air compressor with HILF1 had an equivalent acoustic power of about 110 hp (1700 ft^3/min at 5 psig) and an impedance of about 120 kΩ. By switching to a centrifugal blower for the dc air supply, we expect to increase the available acoustic power in the dc flow to 220 hp (3400 ft^3/min at 15 psig) at an impedance of 60 kΩ. We anticipate that with this source replacement, the sound intensity in the HILF2 chamber could be increased 10 dB over the HILF1 design.

3.2.2 Energy Transfer

Experiments with the HILF1 design showed that a substantial amount of the energy available in the dc airflow is not transferred into the chamber. If we think of our acoustic source in electrical terms, our problem is similar to a classical pulse power design problem: We have a high-voltage (pressure), low-current (airflow limited) power supply with a high average power and we need to drive a low-impedance load with a high current (flow). We can maximize the amount of available power delivered to the load by dc charging a storage capacitor (chamber volume) and then quickly discharging the capacitance through a low-impedance output switch when the storage capacitor has stored all of the available energy delivered by the source per period. By discharging the storage capacitor through a low-impedance switch (modulator) we would pick up a substantial sound pressure increase by minimizing the impedance mismatch between the source and the load. As noted in [1], the Wyle modulator used for the HILF1 tests had an effective flow resistance of about 70 kΩ; at resonance, the chamber presents a load of about 2 kΩ (based on the chamber loss estimated from our measurements) to this source impedance. These two impedances act as a voltage divider that reduces the chamber pressure variation (acoustic amplitude) to about 1/35 of its source value. A lower impedance flow modulator and storage surge tank should deliver energy much more efficiently to the chamber.

Designing a low-impedance modulator involves two opposing concerns: the need to maximize the port area available to the airflow and the need to maintain tight tolerances between the large rotating members. A reasonable compromise between these two factors limits the effective area to less than 100 sq. in., which equates to equivalent impedance of approximately 2 kΩ—a good match to the chamber. We anticipate that a new lower impedance modulator and surge tank could increase the SPL by 6 dB.

The surge tank has the added benefit of permitting a reduction in the modulator duty cycle (ratio of modulator ON (open) time to OFF (closed) time), which increases the peak pressures in the storage tank and therefore the airflow pulse released into the chamber. Since our chamber is resonant, wideband pressure impulses released into the chamber will excite this resonance (with variable efficiency), regardless of its frequency. The chamber resonance would be most efficiently excited by a modulator duty cycle of 0.5. However, modeling of the system led to the suggestion that using a low-impedance modulator with a duty factor of 0.3 to release pressure impulses into the chamber from a surge tank could amplify the maximum airflow from its dc value of 3400 ft^3/min to peak flow impulses in excess of 10,000 ft^3/min. We anticipated that these changes would increase the average SPL by an additional 3 dB.

3.2.3 Acoustic Efficiency

As mentioned in section 1.1, the performance of the HILF1 systems is strongly determined and limited by acoustic losses—particularly since the systems rely on resonance and therefore depend upon storing acoustic energy in the system. In [1], we postulated several acoustic loss mechanisms and described experiments to quantify these losses. In addition to the calculated wall absorption (which, as we have seen, was inadequate to explain our results), these mechanisms included wall flexure and unidirectional airflow through the port. Two additional mechanisms are (1) chamber leaks, and (2) port mass loss at high sound intensities.

Chamber leaks are simply holes through which sound may escape the chamber. Since the HILF chambers are large and have a number of openings and joints that must be sealed for optimum operation, leaks of some size are certain to exist and are expected to be difficult to quantify.

A drawback of the HILF1 design is that the air from the compressor and modulator must flow through the chamber to free space via the tuning port. This creates a substantial wind in the chamber, which may interfere with human or biological effects experiments. Port mass loss caused by dc airflow through the port has been mentioned and was discussed briefly in [1]; simply put, a substantial unidirectional airflow through the port or vent may blow the reactive air mass in the port or vent out of the system, carrying sound energy in the form of SPL-driven air-particle velocity with it. An

estimate of the impact of this effect on system performance is presented in appendix C. The two-volume HILF2 eliminates this loss by eliminating the dc airflow through the port. However, at sufficiently high SPL, a second, similar energy loss may be driven by the sound itself; that is, substantial movement of air through the port is driven by the sound pressure. If the effect is real, we expect it to be nonlinear and to become important at a critical SPL. An estimate of the SPL at which this effect should become significant is also presented in appendix C. As discussed there, this loss may be reduced by altering the port or vent dimensions to increase its volume without increasing its acoustic mass.

4. Development of the Second-Generation High-Intensity Low-Frequency Source (HILF2)

HILF1 was a proof-of-principle experiment and feasibility demonstration. Our overall goal for HILF2 was to design, build, and test an infrasonic test system that would be a deliverable, useful system for conducting acoustic effects experiments. HILF1 was a temporary test system: The air source and modulator were borrowed and not available for long-term use. The concrete chamber was located in a field at the ARL Blossom Point Test Facility; no shelter was available and neither provisions for, nor permission to carry out, long-term materiel and biological effects experiments were provided. In addition, to the extent possible, we wanted to correct some of the performance deficiencies found in the HILF1 experiments. Therefore, we identified the following tasks for designing, constructing, and testing HILF2:

(1) Redesign the test chamber to reduce acoustic losses and minimize airflow problems.

(2) Reconfigure the system to use a new, dedicated, higher horsepower, lower impedance compressed air source.

(3) Design and construct a new flow modulator with a variable duty factor that could be coupled to a surge tank to allow the chamber to be driven by high-intensity wideband flow impulses and thereby maximize the sound intensity in the chamber.

(4) Integrate the components to produce a reasonably portable and reliable system capable of being moved to an offsite research facility and used in long-term acoustic effects experiments.

(5) Conduct a series of experiments to characterize the performance of the system and generate procedures and guidelines for its operation.

In the following sections, we describe the modeling and test of a new design concept for the chamber/resonator (sect. 4.1), the new air source used for HILF2 and its performance characterization (sect. 4.2), the modeling and construction of a new flow modulator (sect. 4.3), and the modeling of the overall performance of the new system (sect. 4.4).

4.1 Two-Volume Helmholtz Resonator Test Chamber

As noted briefly in section 3.2.3, the HILF1 chamber/resonator design required the unidirectional (dc) component of the airflow from the modulator to pass through the chamber and out the tuning port, causing possible acoustic losses and posing a potential "wind" problem for a system user. For the HILF2 design, the increased source capacity and modulator flow would exacerbate this dc flow problem.

Our solution to this problem is to use a two-volume design for the acoustic chamber. In this design, the first volume receives the ac and dc airflow from the modulator and a vent is included that allows only the dc portion of the airflow to escape to free atmosphere. The ac SPL from this volume is coupled through a tuning port to a second, sealed test volume; this effectively eliminates dc airflow through the tuning port and within the test volume. Figure 2 shows this arrangement, which is the idea behind the HILF2 two-volume Helmholtz resonator. The electrical circuit analog to this system is shown in figure 3. The tuning port is now a duct connecting two volumes ("input" and "test") separated by a rigid partition in the chamber. The two volumes act as two compliances, C_{v1} and C_{v2}, in series (through "ground") connected by the port mass, M_p; thus, the undamped resonant frequency, ω_0, of the combined volumes is given by

$$\omega_0 = 1/(M_p C_{eff})^{1/2}, \tag{1}$$

where

$$C_{eff} = C_{v1} C_{v2}/(C_{v1} + C_{v2}). \tag{2}$$

Airflow from the compressor and modulator with its ac (acoustic) and dc (average unidirectional flow) components enters the input volume. The ac component excites the chamber resonance, causing a pulsating airflow in and out of the test volume with no net dc component. Thus, no unidirectional "wind" exists in the port or the test volume. The dc flow component escapes the chamber via a vent opening into the input volume (fig. 2). This vent is chosen to be a long (20 ft) pipe of moderate diameter (8 in.) and, consequently, has a large acoustic mass, M_v. By virtue of its large mass, this pipe presents high impedance to the acoustic signal in the chamber but allows the dc airflow component to pass out of the system (fig. 3).

4.1.1 Modeling and Proof-of-Principle Experiment

We explored the expected response of the two-volume Helmholtz system using the electrical analog model of the system shown in figure 3. The various elements used in the ac circuit analysis are described in detail in appendix A. Initial modeling results indicated that the concept was viable, and we planned an experiment to further test the concept.

We modified the HILF1 chamber by installing a heavy plywood partition from floor to ceiling across the long dimension of the chamber. This partition separated the chamber into two volumes with height and width of 5 by 5 ft. and with depths of 36 1/4 in. and 42 1/2 in., respectively, for the input and test volumes. To anchor and further stiffen the partition, we attached it with U-bolts to two 1-in.-diam. steel rods that passed through the center of the chamber. One rod was attached to steel plates in the center of the cham-

Figure 2. Block diagram of proposed acoustic test system with the use of a two-volume Helmholtz resonator.

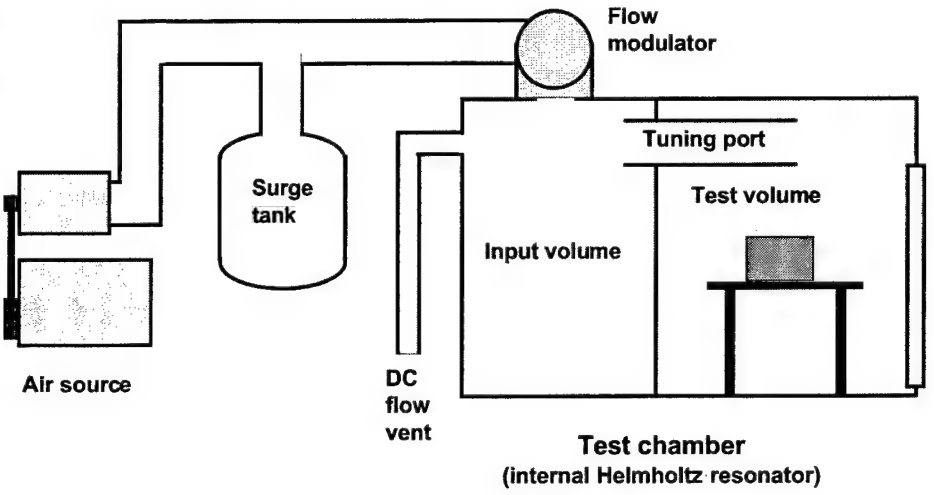

Figure 3. Electrical circuit analog for the two-volume Helmholtz resonator acoustic test system.

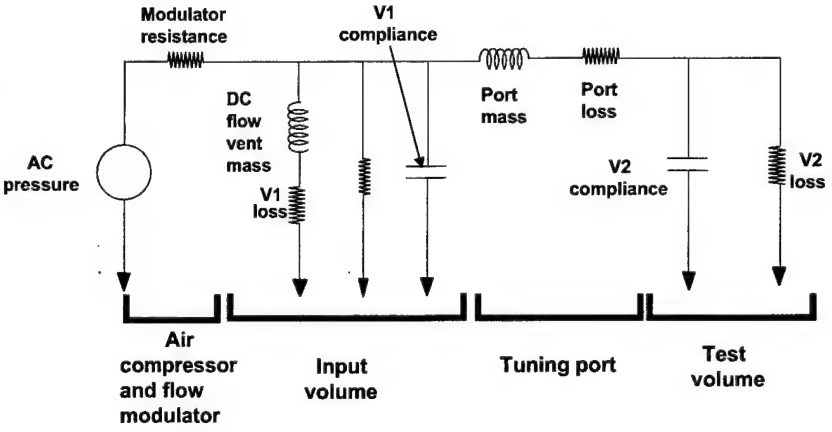

ber lid and bottom; the other was attached to plates near the midpoints of the long sides of the chamber. (These rods had been installed for chamber stiffening in previous experiments; see [1].) For the tuning port between the chambers, a 10-in.-diam. PVC pipe coupler was mounted in a hole in the partition to take various lengths of 10-in. internal diameter PVC pipe. Each of the chamber volumes had a 2-ft.-diam. access hatch in the chamber lid. As for the HILF1 tests, the MOAS flow modulator was mounted at the access hatch to the input volume. In those tests, the tuning port was mounted at the other access hatch; for this experiment, the hatch to the test volume was sealed. An 8-in.-diam. hole was cut in one side of the input volume near the floor and an adapter was mounted in this hole to take 4-in. corrugated plastic drain pipe to serve as the dc flow vent. All gaps and joints in the system were sealed with the use of foam-in-place polyurethane foam sealant.

Figure 4 shows representative modeling and experimental results for the HILF chamber modified as described and with the use of a 10-in.-diam., 27 1/2-in.-long tuning port with a 4-in.-diam., 10-ft.-long dc vent. The smooth curves are model results. For the model, we assumed 6 psi dc pressure input from the MOAS air compressor and 100 percent modulation of this airflow by the MOAS/Wyle 3000 modulator. The two-volume system shows two response peaks. The peak near 12 Hz is the desired chamber resonance that is controlled primarily by the tuning port; the very low-frequency peak below 2 Hz is a system resonance determined primarily by the mass of the vent. As noted in the figure, the four model curves correspond to different values for the chamber acoustic loss, K_{abs}. The upper curve was calculated with the use of the frequency-dependent wall-absorption term described in [1]; the lower curves use successively larger fixed-loss terms. Larger values of K_{abs} result in *lower* values of the parallel loss resistance (fig. 3) and a lower Q associated with the system resonance. Based on our previous experimental results from HILF1, we anticipated chamber losses corresponding to K_{abs} = 0.03 and a system Q near 4.

To measure the response of the two-volume chamber, we used the same techniques and instrumentation as described in [1] for characterizing HILF1. A microphone was placed in the approximate center of the test volume, the acoustic signal from the MOAS source was swept from 0.3 to 20 Hz in 80 s, and the acoustic signal was recorded in digital form. We generated frequency response curves for the chamber by performing a fast Fourier transform (FFT) on the frequency sweep data. The ragged curves in figure 4 are the FFT results for frequency sweeps run at 6 psi and 12 psi dc air pressure input for the lower and upper curves, respectively. As can be seen in the figure, the two-volume chamber behaved qualitatively as expected. The measured resonant frequency, f_{res}, of the system in both cases was 11.7 Hz, in reasonable agreement with the model predictions (e.g., f_{res} = 12.2 Hz for

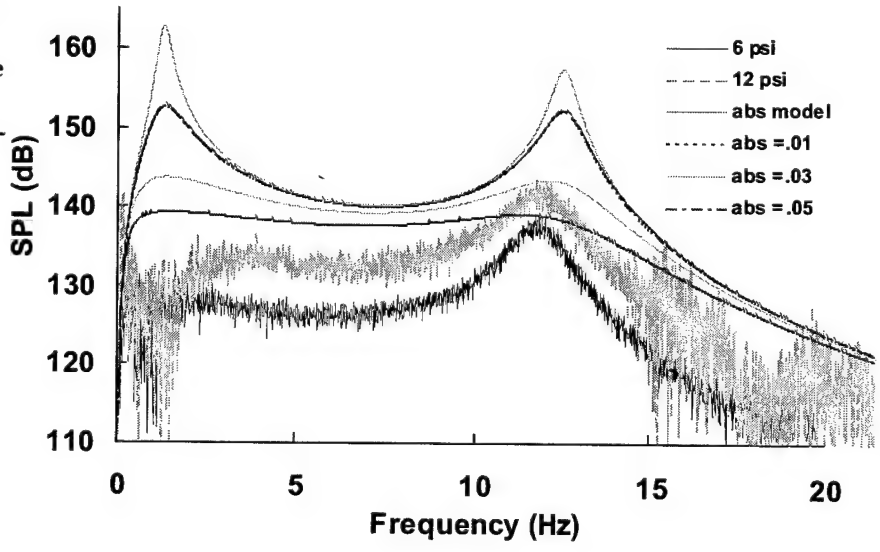

Figure 4. Predicted and measured frequency response of two-volume Helmholtz resonator system used in proof-of-principle test. Smooth curves are predicted response assuming various acoustic losses (see text). Ragged curves are measured responses at 6 psig (black) and 12 psig (gray) input dc air pressure.

K_{abs} = 0.01). However, the SPL we observed in the test volume was substantially less than predicted—138 dB at f_{res} for 6 psi input versus a predicted value near 146 dB for K_{abs} = 0.03. This indicates that the overall system losses were greater than expected. In apparent contradiction, by comparing the shapes of the response curves in figure 4, we can see that the measured resonance peak is actually sharper (higher Q) than the model curve for K_{abs} = 0.03 and more closely agrees with the K_{abs} = 0.01 curve. This implies that the measured chamber losses are actually *less* than predicted. Apparently some mechanisms other than chamber loss reduced the chamber SPL below expectations. One candidate is dc backpressure in the chamber caused by restricted airflow through the vent. During the course of the experiments, we observed that the concrete access hatch on the test volume tended to lift up while the air source was running. The hatch consists of 5-in.-thick concrete; its weight per unit area corresponds to a pressure of about 375 kg/m^2 or about 0.5 psi. Evidently, the 4-in.-diam. dc vent was too small to handle the airflow from the modulator.

4.2 DC Air Source: Dual Centrifugal Compressors

The best dc air source for our effort would be one with the lowest equivalent impedance; that is, it would have the highest flow rate while maintaining moderate back pressures (<15 psig). These requirements lend themselves to the use of a centrifugal-type air pump (centrifugal blower). Centrifugal blowers can typically maintain high flow rates at good efficiencies (>50%) and have the added advantage of being very compact. These characteristics make centrifugal blowers an ideal choice for superchargers on high-performance engines. When selecting the manufacturer of the centrifugal blower, we focused on the automobile industry since by far the bulk of the R and D in this technology has focused on optimizing blowers for racing. The blower we selected was a Paxton Novi-2000 model supercharger with a manufacturer's specification of 1700 ft^3/m at 28 psig. The Novi-2000 is a high-efficiency (almost 70 percent) belt-driven pump that is <12 cu. in. in volume. For our infrasonic source, we decided to use two superchargers in parallel for a total available airflow of 3400 ft^3/m.

To power the superchargers, we used a "big-block" high-performance Chevrolet racing engine modified to provide approximately 400 hp. A big-block engine was chosen since it is known for its broad torque vs. rpm curve (at the expense of limited high-end rpm). Since we wanted to be able to run the engine through a wide range of speeds, we believed that it was important to use an engine with a broad torque response rather than one that would have to run at maximum rpm at all times to achieve the power output we required. After selecting the air source components, ARDEC let a separate contract for the purchase and integration of the dual superchargers and racing engine. The delivered source consisted of the superchargers mounted on the front of the engine and driven from the front crankshaft pulley with 10-rib serpentine belts. The entire engine-compressor system

was mounted on a commercial engine test stand together with supporting subsystems (engine control, ignition, charging, and cooling systems).

Since a centrifugal blower transfers energy to the airflow through the velocity of the tips of the impeller fins, the rpm of the impeller determines the output flow rate. The Paxton superchargers are each rated by the manufacturer to produce a flow, F_c, of 1700 ft^3/m and a pressure, P_{max}, of 28 psig at a maximum impeller speed of 50,000 rpm. Although the backpressure claim of 28 psig seemed a bit optimistic, we felt that we could safely reach our target backpressure of 15 psi.

For two compressors developing both maximum flow and maximum pressure simultaneously, the power input to the airflow, $F_c P_{max}$, is 310 kW or 410 hp. The engine was expected to be capable of developing about 400 hp at 4000 rpm. In an ideal centrifugal blower, the flow volume varies directly with impeller rpm and the static pressure varies as the square of the rpm. These relationships are shown in figure 5 for the flow volume and in figure 6 for the static pressure (solid lines).

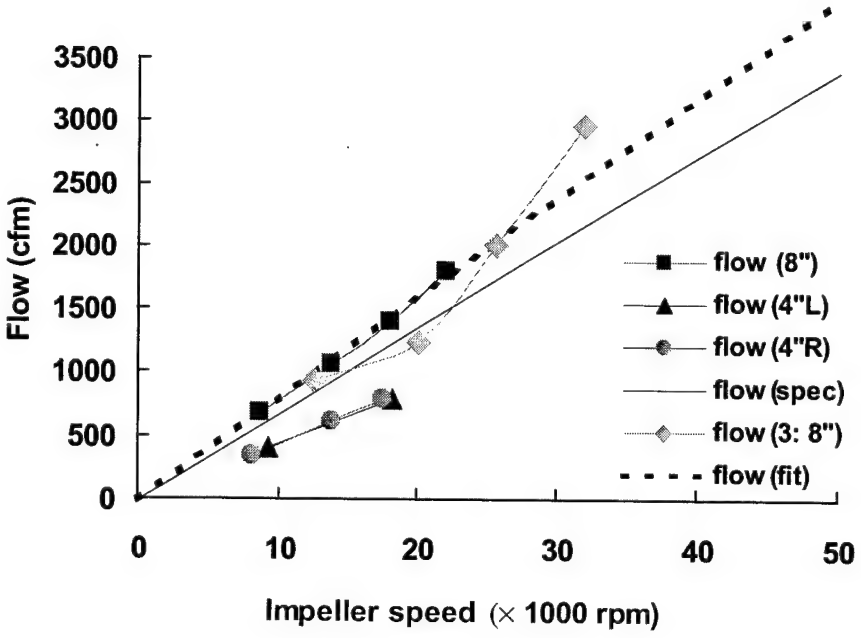

Figure 5. Airflow as a function of impeller speed for dual Paxton compressors. Data points are measured flow; solid straight line is specified flow, and dashed straight line is best fit to measured flow.

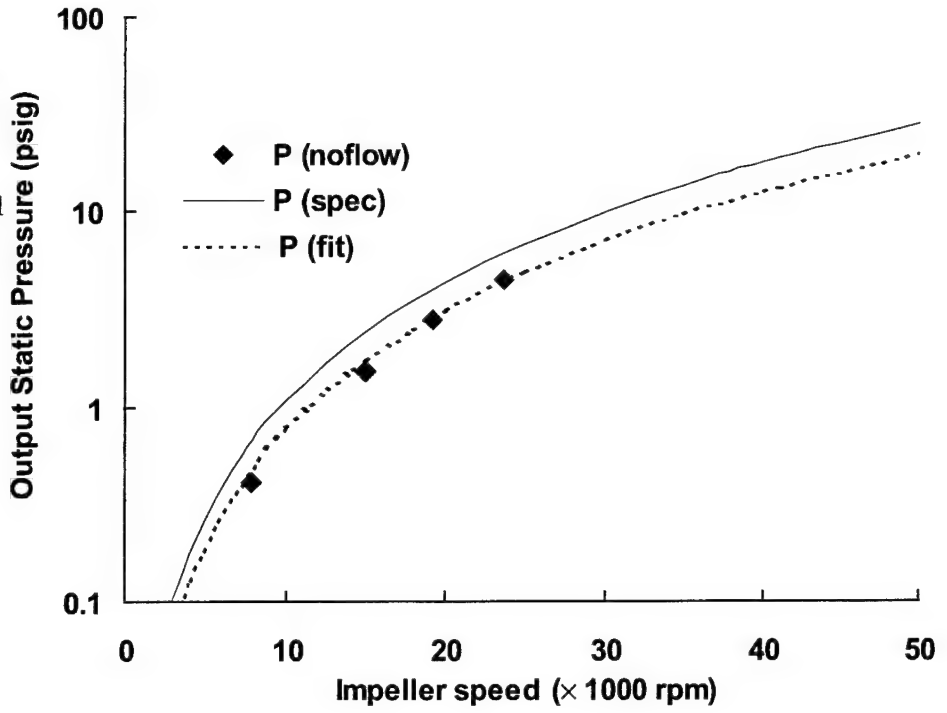

Figure 6. Output pressure with flow blocked as a function of impeller speed for dual Paxton compressors. Solid line is specified output pressure; dashed line is square law fit to measured pressure.

4.2.1. Supercharger Limitations

The air source (engine and superchargers) as delivered used 8-in.-diam. crank pulleys and 3-in.-diam. pulleys on the superchargers. The Novi-2000 has an internal gear couple of 3.54 for a total ratio of 9.44:1 from crank to blower impeller. This compressor drive pulley ratio did not allow us to drive the compressors at their maximum rpm and thereby realize their full capacity. To reach the Paxton optimum speed of 50,000 rpm, the engine would need to turn at almost 5300 rpm. We believed that this was an excessive speed for continuous operation of a big-block engine. We were unable to determine the specified maximum rpm at which the engine could be run continuously, so we estimated this limit to be 4000 rpm. To use more of the capacity of both the compressors and the engine, we altered the drive pulleys. First, we replaced the 3.5-in. pulleys on the Paxtons with smaller, 2.25-in.-diam. pulleys. With the original crankshaft pulleys, the new units were expected to increase the maximum compressor impeller speed from 38,000 to 50,000 rpm at 4000 engine rpm. Unfortunately, the serpentine belts began to slip on the small pulleys at about 2500 engine rpm, so the maximum impeller speed was again limited to about 38,000 rpm.

To correct the belt slippage limitation, we went back to the original 3.5-in.-diam. pulleys supplied with the supercharger and increased the diameter of the crank pulleys to 12 in. to maximize contact surface on the belt and

still achieve the pulley ratio needed to properly drive the superchargers. Again the belt began to slip at an impeller speed of approximately 38,000 rpm. As mentioned earlier, the output flow is proportional to rpm and the pressure is proportional to the square of the rpm. This means that the horsepower required is proportional to the cube of the rpm! At higher speeds, a small change in rpm corresponds to a substantial increase in required horsepower. It appears that the 10-rib belt supplied with the superchargers was unable to transfer the hp required to drive the superchargers to their rated value.

4.2.2 Experimental Evaluation

Figures 5 and 6 also show the results of flow and pressure measurements taken with the compressor system operating with the original 2.43:1 pulley ratio. We measured airflows with an Omega Engineering FMA-906-V thermal air velocity sensor placed in either of the 4-in-diam. PVC pipes that connected the output of the Paxton blowers to the surge tank or in one of the 8-in.-diam. output vent pipes that exhausted the dc airflow from the chamber input volume. In figure 5, measured flow from the Paxtons is designated as 4" L or 4" R corresponding to the outputs of the blowers located on the left or right side of the engine as viewed from the front (radiator). The flows from the two compressors were reasonably well matched. The chamber output flow (8 in. in the figure) was measured with a single vent open. Note that the total output flow measured in the 8-in. vent was noticeably less than the sum of the Paxton outputs at higher impeller speeds (i.e., about 1400 ft^3/m versus 2×750 ft^3/m at about 1750 rpm). We attribute the difference to leakage from the various joints in the chamber and its connections. Note also that, despite the leaks, the no-load total flow from the compressors exceeds the specified flow.

We measured compressor output and surge tank pressures with Omega engineering PX235 current-loop pressure transducers. The compressor zero-flow output pressure measurements shown in figure 6 were obtained from a transducer mounted on one of the Paxtons' 4-in. output pipe; the measurement was performed when the pipe was momentarily blocked. The measured pressures were about 30 percent lower than given by the idealized specified performance curve.

4.3 Low-Impedance Flow Modulator

To optimize the energy transfer from the dc air source to the chamber, we planned to use the air source and a low-impedance flow modulator to cyclically "charge" or pressurize a storage tank and then rapidly discharge the storage tank into the chamber as a series of airflow impulses. Since HILF2 is a resonant chamber, it operates at a single frequency, f_{res}, predetermined by tuning, and it cannot reproduce an arbitrary waveform. It will respond to, and amplify, acoustic energy from the flow modulator that falls within its

resonance bandwidth, and, as long as substantial acoustic energy from the source exists at f_{res}, the dominant signal present in the chamber will be a sine wave with frequency f_{res} *regardless* of the input waveform. Thus, we can, for example, excite the chamber with a series of pulses having a repetition rate $1/f_{res}$ and, by virtue of the chamber resonance, expect to obtain a reasonably pure sinusoidal waveform in the chamber.

4.3.1 Low-Impedance Flow Modulator Design

Our goal was to impulsively drive the chamber with the highest flow rates that were feasible. This meant that we needed to design a modulator with an extremely low impedance—preferably on the order of the chamber impedance during resonance (2 kΩ) with a duty factor (fraction of time the modulator is ON (open)) less than 0.5. The impedance of a flow modulator is determined primarily by the effective area of the opening it presents to the flow when it is ON. The MOAS/WAS 3000 modulator had a maximum opening of 3.8 in.^{2}; at 6 psig input, the maximum flow was about 1200 ft^3/m and the effective modulator impedance (incremental pressure/incremental flow) was about 70 acoustic kΩ. To reduce the modulator impedance to about 2 kΩ (rough match to chamber losses), we would need to increase the area to about 50 sq. in. In addition, the WAS 3000 was a voice-coil-actuated modulator normally used to *linearly* vary airflow as a function of an arbitrary audio electrical signal; that is, for a sinusoidal excitation, its opening would vary sinusoidally from fully closed to fully open. This linear mode of operation is, at best, about 50 percent efficient in the use of power in the airflow. The new modulator would operate in the more efficient manner of a nonlinear switch and drive the chamber with airflow impulses.

The largest practical port area was determined mainly by the mechanical limitations of building the modulator (i.e., large ports require a large frame that must be rotated a high speeds while maintaining close tolerances between the rotating surfaces to minimize air leakage). The total port area chosen for the modulator was 70 in.^{2} (two 12-in. × 2.9-in. slots). The acoustic impedance represented by this aperture is dependent on pressure across the aperture but should be on the order of 2 kΩ.

Figure 7 shows the principle behind our design for a large-area pulsed flow modulator. The modulator consists of three closely spaced coaxial cylinders. The inner and outer two cylinders (stators) are fixed; the middle cylinder rotates freely with respect to the stators forming what is sometimes called a "captive rotor." The use of pilot and thrust bearings on the rotor allows tight tolerances (typically 0.003 in) between the rotating surfaces and translates forces to the modulator case and away from the rotor. The rotor has two diametrically opposed slots parallel to its axis; their combined area is the maximum flow area of the modulator (70-in.^{2}). The stators have similar axial slots that are twice the width of the stator slots. One of the stators can be rotated slightly with respect to the other to vary the overlap of the

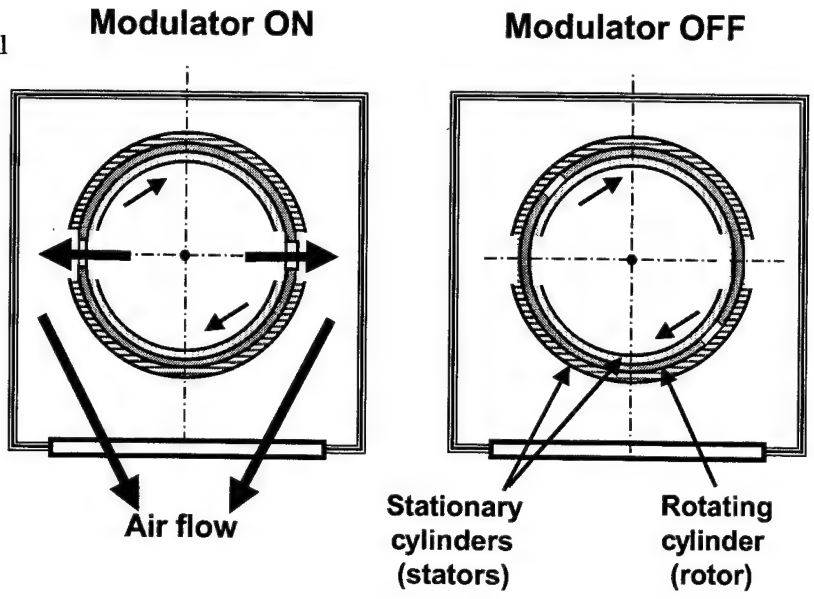

Figure 7. Principle of captive-rotor cylindrical coaxial rotary-flow modulator.

stator openings. This assembly forms a rotating valve. The modulator is mounted directly to the storage tank to minimize loss. Air under pressure is admitted to the cylinders along the axis at one end.

The inner stationary cylindrical stator is completely sealed except for the two aperture slots. This feature has a significant effect on the mechanical efficiency of the valve. In a typical rotating air valve, the rotor is exposed to the static load from the dc air pressure and the dynamic load created by the pulsating air. This is not a trivial load; the authors have evaluated sirens using 2-hp motors to spin the rotors that have either seized or were unable to maintain frequency stability due to these forces. To compensate for these loads, the tolerances between rotating surfaces must be relaxed, or increased power is required to turn the rotor and sophisticated feedback control is required to maintain frequency stability. Relaxed tolerances also permit air to leak from the modulator and decrease its acoustic efficiency. Another source of decreased acoustic efficiency is the imparting of spin to the air inside the valve by the rotor. This air rotation creates turbulence that impedes the normal airflow in the valve and contributes to the valve's impedance. The captive valve design described here minimizes each of these effects. Since the inner stator is sealed, nearly 76 percent of the inner rotor surface is isolated from the incoming air. This in effect reduces the radial forces on the rotor and circular turbulence by that amount and completely eliminates axial and dynamic forces.

The rotor is spun by an electronically speed-controlled 2-hp electric motor at $1/2\,f_{res}$ (two slots generate two air pulses per revolution). When the rotor slots move into position between the stator slots, the modulator is ON and

a pulse of air exits the slots and is directed into the HILF chamber. The modulator duty cycle, k_{dty}, is defined as the fraction of the rotational period that the modulator is OFF. The motor used for this application was purchased for another application and is far from optimum for this experiment. The motor is designed to develop 2 hp at 10,000 rpm and provides a constant torque of 1 ft-lb. Since we are interested in acoustic tones in the infrasonic range, the motor is being used far below its optimum speed and will therefore provide only a fraction of its rated power at these lower speeds. To keep the motor rpm as high as feasible, a pulley ratio of 4.74 was used between the valve and the motor. At a nominal acoustic operating frequency of 10 Hz, the corresponding motor speed would be 1422 rpm. This corresponds to only 0.27 hp delivered by the motor. At the lower frequency limit of 2.5 Hz, the power delivered by the motor was less than 0.1 hp: successful operation of the modulator under load at this speed showed that the captive rotor design was mechanically efficient and very effective at minimizing unnecessary forces on the rotor.

To maximize the energy transfer from the dc air source and the chamber, we included in the modulator design the flexibility to "tweak" its operating characteristics. The adjustable stator mentioned above allowed us to vary slightly the maximum port area and the modulator duty cycle. The k_{dty} could be adjusted from 0.3 to 0.5 for a constant peak aperture of 70 in^2. The aperture area can also be varied from fully open to fully closed at an approximately constant $k_{dty} = 0.27$.

4.3.2 Storage (Surge) Tank

The storage tank served two purposes: (1) store the excess air volume (and, consequently, airflow energy) generated by the dc air source during that portion of a cycle when the modulator is closed and thereby maximize the available pressure, and 2) optimize the average acoustic power in the airflow impulse released into the chamber by increasing the duration of the airflow impulses.

Selecting the optimum tank size is a very complicated, recursive process since it is dependent on the air source flow and achievable backpressure, duty cycle of the modulator, impedance of the modulator, and duration of the impulses generated. This problem was further complicated since each of these variables is interdependent on the others. The ultimate objective is to tailor the shape of the impulse released into the chamber so that it contains as much average acoustic power as possible within the bandwidth for which the chamber is tuned. The final volume of the tank was chosen to be 8.9 ft^3 (0.25 m^3), which would allow us to operate at $k_{dty} = 0.3$ (to maximize pressure) and maintain significant energy at the fundamental of the frequency spectrum of the impulse.

4.3.3 Modeling the Performance of the Modulator and Storage Tank

The flow modulator, surge tank, and engine-air compressors function together as the acoustic signal source for the chamber. For purposes of the ac chamber response model, the acoustic source is modeled as an ac pressure source, P_i, in series with a resistance, R_f (the flow modulator impedance) (fig. 3). The P_i and R_f clearly are functions of the pressure and flow characteristics of the whole signal source subsystem. We modeled the output of the signal source by first obtaining estimates of the output pressure and flow volume of the compressors at a chosen engine speed as described in section 4.2; we then applied the resulting compressor dc flow rate, F_c, and maximum pressure, P_{max}, as inputs to the surge tank and modulator with the modulator operating at the chamber resonant frequency f_{res} with a duty cycle k_{dty}. The time-dependent modulator output flow, F_m, and surge tank pressure, P_t, driving this flow were calculated by the use of an *ad hoc* BASIC program that iterated the following difference equation on time steps Δt:

$$P_t(i) = \{[(F_{in}\,\Delta t - F_m\,\Delta t + V_t)/V_t]^{\gamma}\,(P_t(i-1) + P_{atm})\} \;/\; P_{atm}\,,$$

where V_t is the surge tank volume and γ is the adiabatic heat capacity of air. F_{in} was assumed to vary linearly with the input pressure differential; that is, $F_{in} = F_c\,(P_{max} - P_t(i-1))/P_{max}$. F_m is, itself, a function of P_t, the temperature, T_t, of the air in the tank, and the instantaneous area, $A_m(t)$, of the modulator opening. $T_t(t)$ was calculated in parallel with $P_t(t)$:

$$T_t(i) = T_t(i-1)\,[(V_t + F_m\,\Delta t)/V_t]^{1-\gamma}\,.$$

The measured compressor outlet air temperature was used as the initial value for T_t. The k_{dty} was fixed at 1/3 for these calculations (for our measurements, the actual value was 0.3); at this setting, the modulator opening area ramped linearly from zero to its maximum value and back to zero in 1/3 of the modulator period. At each time step, $F_m(t, P_t, T_t, A_m)$ was calculated using adaptations of the expressions previously used to calculate flow through the WAS 3000 flow modulator (see Appendix B).

Figure 8a shows results calculated for several modulator cycles with the modulator operating at a frequency of 12 Hz with inputs F_c = 1800 ft^3/m, P_{max} = 3.7 psig, and input air temperature of 35 °C. The surge tank volume is 8.9 ft^3. Figure 8(b) is a detail of a single modulator output pulse. The dashed lines represent the flow modulator opening area. The airflow through the modulator peaks at about 3.3 m^3/s and then starts dropping before the modulator reaches full opening. The tank pressure varies from about 2.6 psig just before the modulator starts to open to less than 0.1 psi soon after the modulator reaches full opening. The resistance, R_f, of the modulator varies from infinity to some minimum value as the modulator opens up, so the choice of a proper single value for R_f is not obvious. Since the maximum signal input to the chamber corresponds to the maximum flow, we defined R_f to be the tank pressure at the time of maximum flow divided by the maximum flow. For the present case shown in figure 8(b), P_t = 1.0 psig when F_m peaks at 3.3 m^3/s, and R_f = 1 psig/(3.3 m^3/s), or 2120 acoustic ohms in

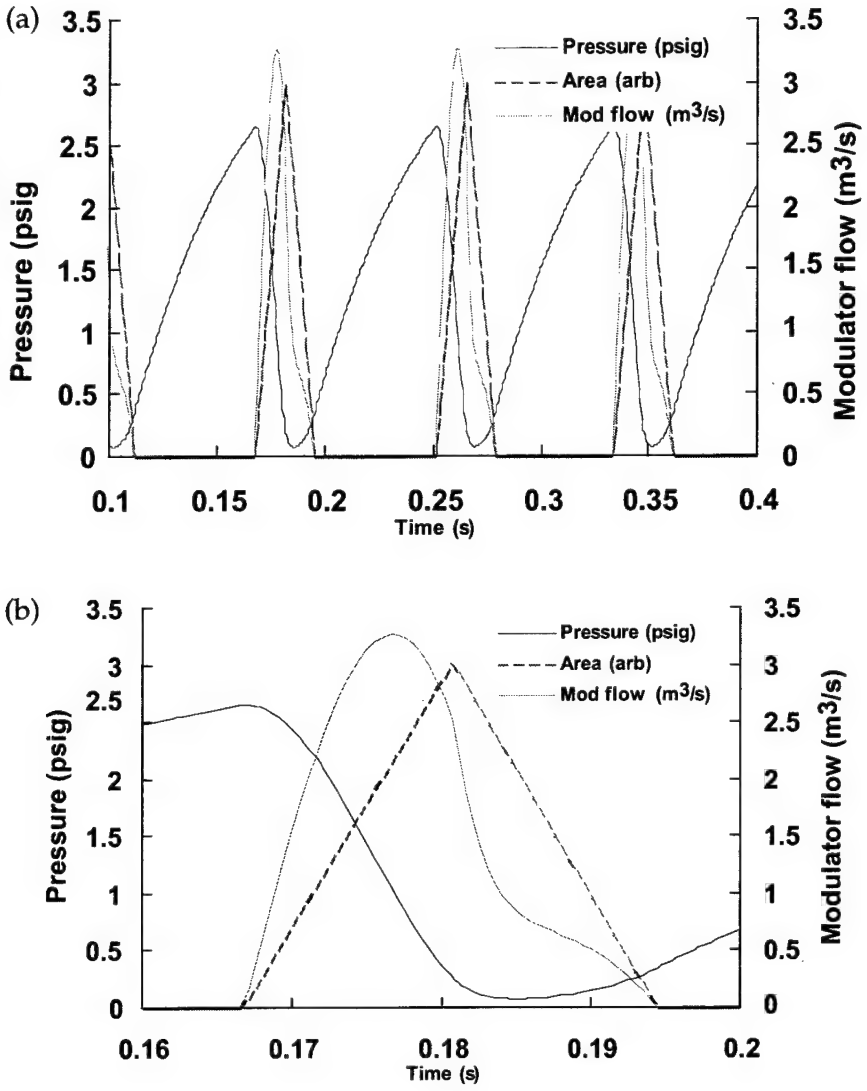

Figure 8. Calculated pressure and flow as a function of time in flow modulator-surge tank system operating at 12 Hz with input F_c = 1800 cfm and P_{max} = 3.7 psig. (a) Several modulator cycles; (b) detail of a single modulator pulse.

consistent units. This value is very close to the modulator design goal of 2000 Ω.

To determine that portion, F_{rms}, of the acoustic power contained in the airflow pulses from the modulator that is effective in exciting the chamber resonance, we performed a fast Fourier transform (FFT) on $F_m(t)$ after first removing the dc flow component and calculating the total rms value of the waveform $F_m(t)$ at all frequencies, F_{trms}. Figure 9(a) shows the resulting acoustic spectrum for the modulator. From the figure, the spectral peak at the modulator fundamental frequency of 12 Hz has an amplitude of about 0.65 m^3/s. Since the power associated with a spectral peak is a function of its width as well as its amplitude, we obtained a more correct value by examining the cumulative integrated power spectrum as shown in figure 9(b). The system will be driven effectively by that fraction of the acoustic power that falls within the resonance bandwidth. Assuming a Q of 3, the bandwidth at 12 Hz is 4 Hz and the system will respond to energy in the range

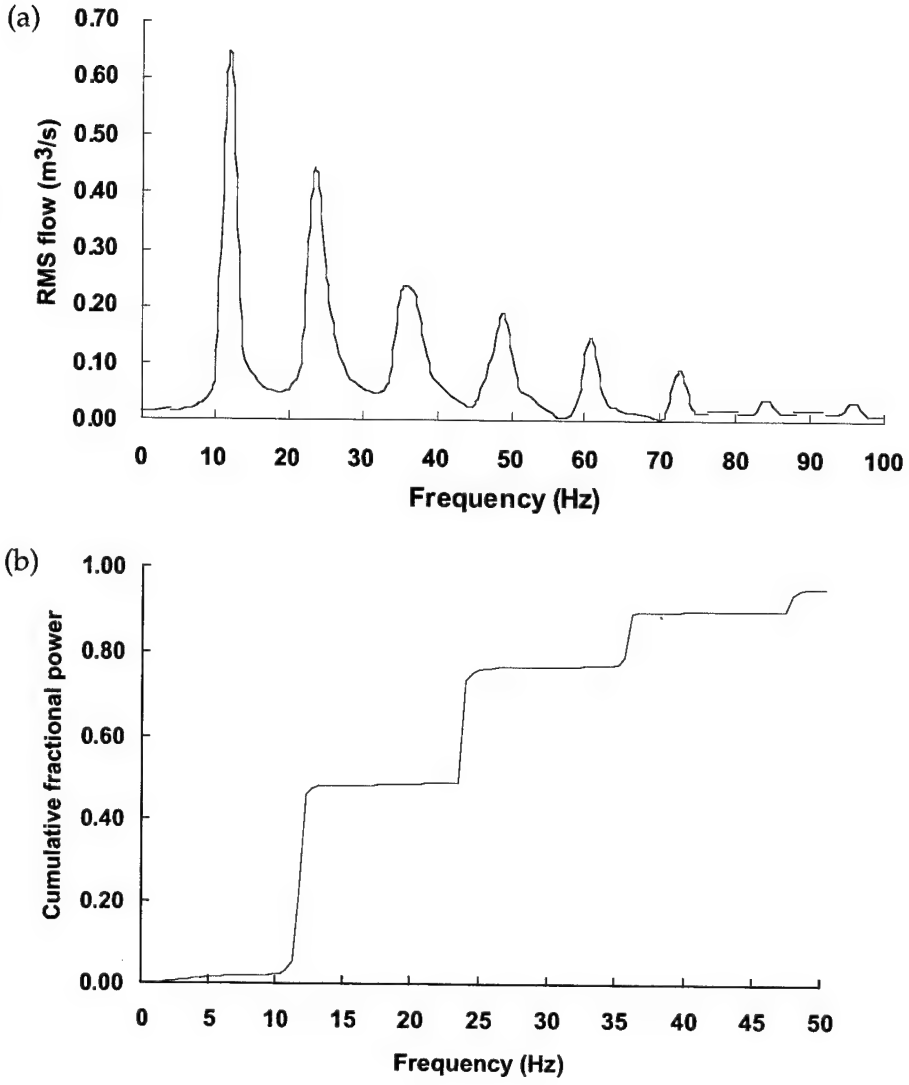

Figure 9. Acoustic power in modulator pulses as a function of frequency obtained from fig. 8 by FFT. (a) Flow spectrum; (b) cumulative acoustic power as a function of frequency.

from 10 to 14 Hz. For our example, from figure 9(b), a fraction $k = 0.46$ of the acoustic power in the flow falls in this range. For this case we also have $F_{trms} = 0.97$ m^3/s. The total power in the flow is proportional to $(F_{trms})^2$; therefore, the rms amplitude of the effective fraction of the modulator spectrum is $(F_{rms})^2 = k\,(F_{trms})^2$ or $F_{rms} = (0.46)^{1/2} * 0.97$ m^3/s = 0.66 m^3/s—a very small correction to the peak value read from figure 9(a). The equivalent ac rms source pressure at the modulator fundamental frequency, P_i, that would drive this flow through the modulator resistance, R_f, is

$$P_i = F_{rms}\, R_f\,.$$

Therefore, for this case the equivalent circuit elements for the modulator are R_f = 2120 Ω and P_i = 0.66 m^3/s * 2120 Ω = 1400 Pa at f = 12 Hz.

Based on early measurements of the performance of the supercharger system that used the 2.25-in.-diam. pulleys on the superchargers, we estimated that this system would produce F_c = 2350 ft^3/m and P_{max} = 13 psi at a reasonable maximum engine speed of 4000 rpm. Figure 10 shows the calculated modulator tank pressure and flow for these values of F_c and P_{max} with the modulator operating at 12 Hz; figure 11(a) shows the resulting modulator flow spectrum and 11(b) shows the integrated power in the spectrum. With these inputs, the equivalent circuit elements for the modulator and air source at 12 Hz are F_{rms} = 1.12 m^3/s, R_f = 2472 Ω, and $P_i(t)$ = 2770 Pa. Similarly, figures 12, 13(a), and 13(b) show the calculated source system performance at 4000 rpm with the modulator operating at 5 Hz. In this case, F_{rms} = 0.86 m^3/s, R_f = 4694 Ω, and $P_i(t)$ = 4000 Pa. At 5 Hz, the modulator surge tank has time to "charge" to a higher pressure than at 12 Hz (almost 10 psig vs. 5.3 psig). However, the surge tank empties earlier in the cycle at the lower frequency (well before the modulator reaches full opening), so the effective resistance of the modulator is increased. The modulator is also slightly less efficient at 5 Hz because more of the acoustic energy in the flow pulses it produces is contained in the higher harmonics.

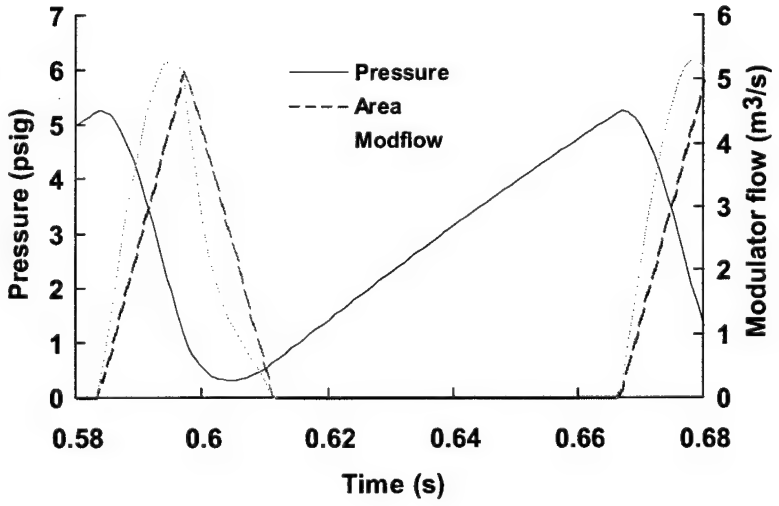

Figure 10. Calculated pressure and flow as a function of time in flow modulator-surge tank system operating at 12 Hz with input F_c = 2350 cfm and P_{max} = 13 psig.

Figure 11. Acoustic power in modulator pulses as a function of frequency obtained from fig. 10 by FFT. (a) Flow spectrum; (b) cumulative acoustic power as a function of frequency.

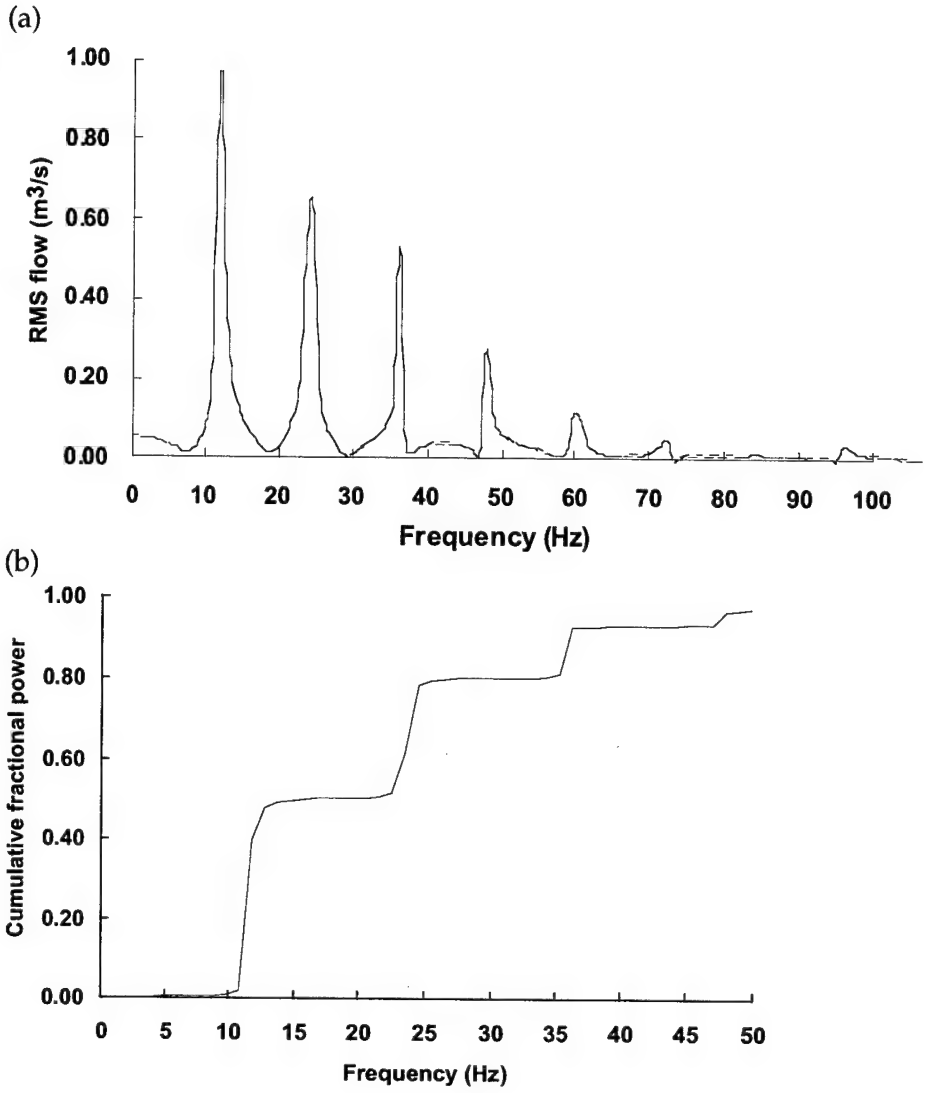

Figure 12. Calculated pressure and flow as a function of time in flow modulator-surge tank system operating at 5 Hz with input $F_c = 2350$ cfm and $P_{max} = 13$ psig.

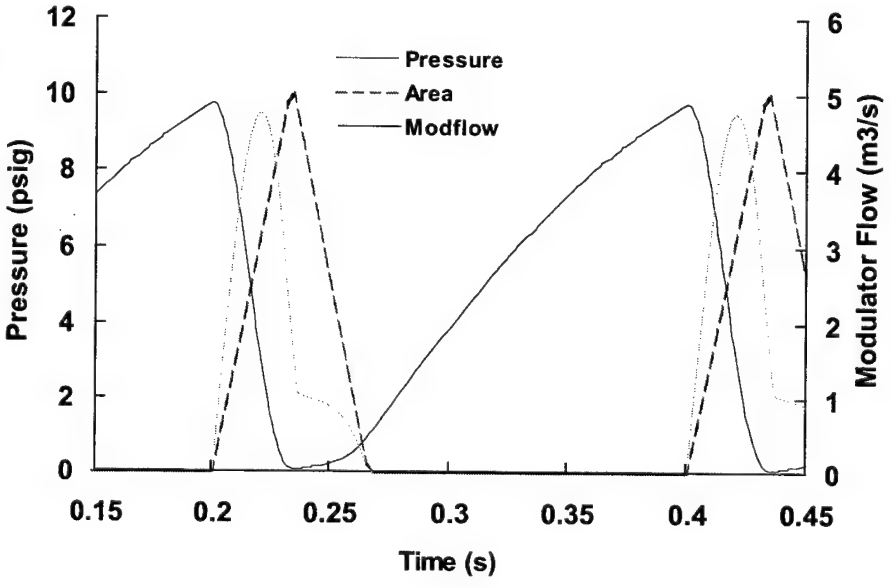

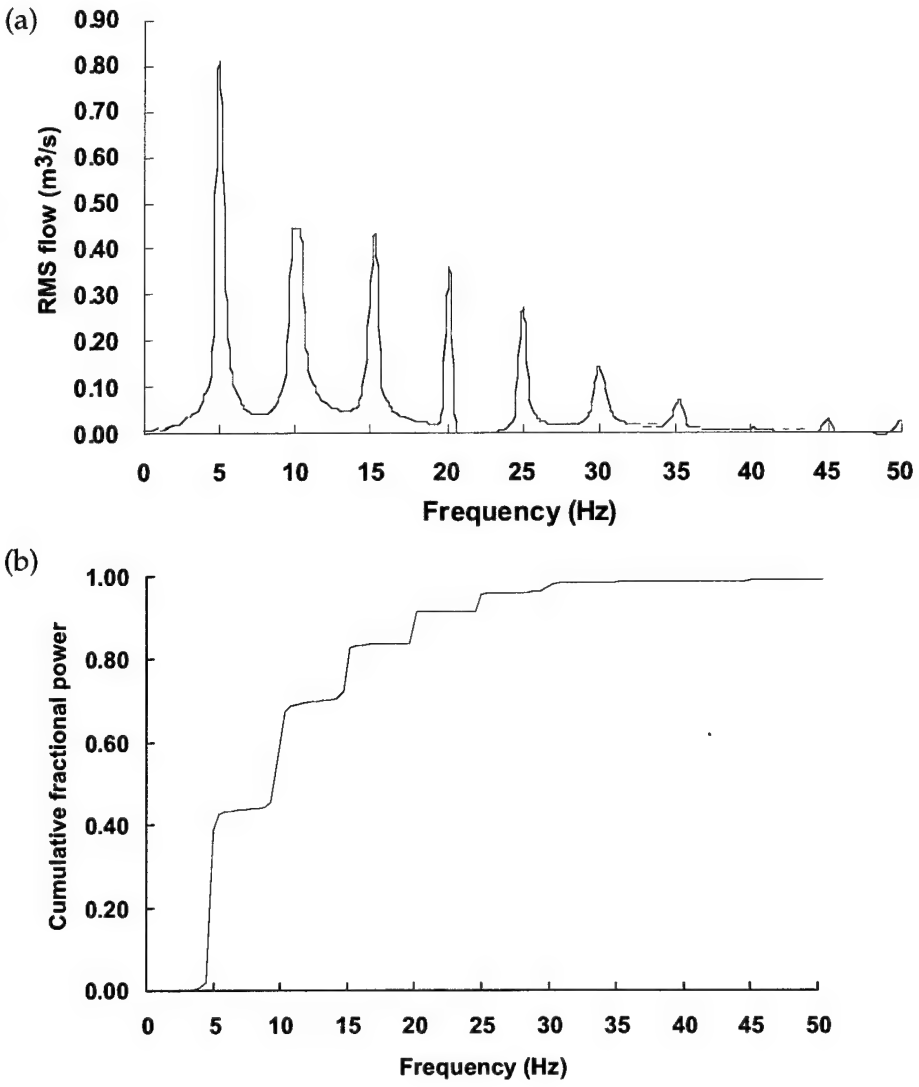

Figure 13. Acoustic power in modulator pulses as a function of frequency obtained from figure 12 by FFT. (a) Flow spectrum; (b) Cumulative acoustic power as a function of frequency.

4.4 Modeling the Performance of the Complete HILF2 System

We next applied the expected acoustic energy output of the air source and flow modulator to our model of the Helmholtz resonator chamber to obtain an estimate or prediction of the overall performance of the second-generation system.

Figure 3 is the simplified circuit model for the two-volume Helmholtz resonator system; the more complete model used for our calculations is shown in figure 14. The major components of the system include the acoustic source represented by $P_i(t)$ and R_f, the input volume (compliance), C_{V1}, and test volume, C_{V2}, and their respective wall-absorption losses, R_{wall}, the internal port with its mass, M_p, compliance, C_p, and loss, R_p, and the vent with its mass, M_v, and loss, R_v. Appendix A gives the general expressions for these acoustic elements in terms of the various dimensions of the system and

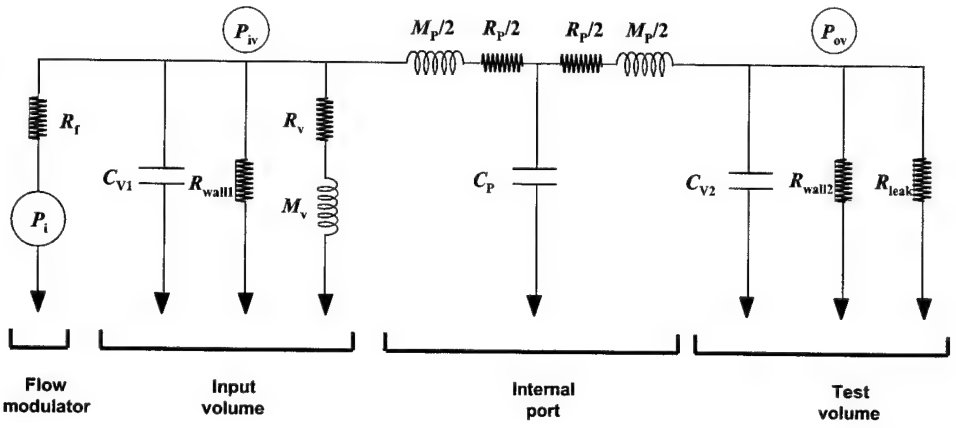

Figure 14. Detailed electrical circuit analog for two-volume Helmholtz resonator acoustic test system.

physical constants. To account for acoustic losses in the chamber in addition to the terms R_{wall} and the port and vent losses, an additional term, R_{leak}, has been included. This loss is added as an air leak from the test chamber and takes the form of a 4-in.-long hole to the outside with adjustable diameter.

We solved the ac circuit loop equations for the circuit in figure 14 by using another *ad hoc* QuickBASIC program that incorporated the (in some cases, frequency-dependent) expressions for the values of the various circuit elements. Outputs from the program were the rms SPLs P_{iv} and P_{tv} for the input and test volumes, respectively, as a function of frequency. Figure 15 shows the calculated P_{tv} response over the range from 0 to 25 Hz for the two-volume system with an 8-in.-diam., 20-ft.-long vent and *two* 10-in.-diam., 54-in.-long internal ports. We planned to use two ports to avoid possible system performance limitation by SPL-induced port mass loss (see app C). We used the values of P_i and R_f calculated for the Paxton compressors operating at F_c = 2350 ft^3/min and P_{max} = 13 psig and with the modulator operating at 12 Hz as discussed in section 4.2. The upper curve in the figure is the test volume SPL calculated with the use of the frequency-dependent wall-absorption losses, R_{wall}. The three curves below include additional loss, R_{leak}, through successively larger leaks with diameters of 0.5, 0.78, and 1.0 in. For this configuration, the model shows a high-frequency resonance, f_{rhi}, at about 13 Hz and a low-frequency resonance, f_{rlo}, at about 2 Hz. The upper resonance is determined by the mass of the internal tuning port and the series compliance of the test and input volumes; the lower resonance is determined by the mass of the vent and the *sum* (or parallel combination) of the two-volume compliances. For our nominal input conditions and the minimum-loss case (no R_{leak}), the model predicts an SPL of 159.4 dB at the upper frequency f_{rhi} = 13.3 Hz; the system Q associated with this peak is 4.56. However, based on our previous experiences with HILF1 and the HILF2 proof-of-principle tests, we were forced to consider this prediction to be optimistic. At 13 Hz, the calculated values of R_{wall1} (input volume) and R_{wall2} (test volume) are 20100 and 18340 Ω, respectively, for a net parallel loss re-

sistance of 9590 Ω. As noted in section 1.2, our proof-of-principle experimental SPL results were best fit with a net parallel loss resistance (chamber impedance) of about 2000 Ω. This net loss can be simulated by the addition of R_{leak} = 2500 Ω, which corresponds to a 0.78-in.-diam., 4-in.-long hole to the outside from the test volume.

The resulting predicted system response is shown in figure 15 (third curve from top). The predicted SPL at f_{rhi} is 155.3 dB with Q = 2.97. Note that a fairly small hole—representing *all* the leaks in the system—reduces the predicted SPL by almost 4 dB.

Figure 15 also shows that the double resonance of the two-volume system produces a band-pass filter response. The system response is predicted to be relatively flat between the two resonant frequencies (within 10 dB with a 0.5-in. leak) with fairly sharp cutoffs at higher and lower frequencies (–20 dB per octave). This suggests that, if maximum SPL is not required, the system can be operated over the range of frequencies in its passband by simply varying the modulator frequency without tuning the port.

Space limitations prevent the use of internal ports in HILF2 with lengths greater than about 60 in. This limits the upper resonance of the two-volume system to frequencies above 10 Hz. (Other system designs that avoid the internal port size constraint will be discussed later.) However, as indicated by the lower resonance in figure 15 associated with the vent, the system might also be operated in a modified single-volume mode. In this mode, the internal port is reduced to a large hole in the partition between the input and test volumes to reduce its mass and raise its associated resonant frequency, and the vent becomes the tuning port. For an 8-in.-diam., 2.5-ft. port coupled with the full chamber volume of 4.5 m^3, f_{rlo} is about 5 Hz. Like

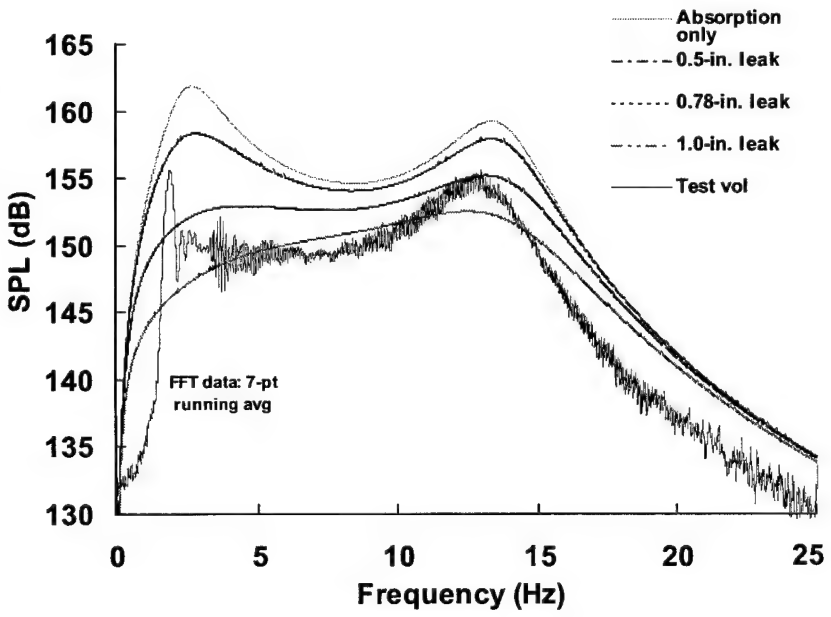

Figure 15. Calculated test volume SPL frequency response in HILF2 with the use of two 10- by 54-in. internal ports and an 8-in. by 20-ft vent and assuming different levels of acoustic loss (see text).

the original HILF1 single-volume Helmholtz resonator system, this arrangement has the disadvantage that the dc airflow component must again pass out of the system through the port. As we discuss in appendix C, the expected losses associated with this flow through the port may limit the system performance. For the single 8-in. port just discussed and a system Q of 3, the criterion developed in the Appendix (eq. C-5) indicates that severe losses will occur for a dc airflow $V_{dcmax} = 262$ ft^3/min—well below the output of the compressors at idle. However, the same f_{rlo} is achievable by the use of *three* 8-in.-diam., 7.5-ft. tubes; this arrangement raises V_{dcmax} to a respectable 2360 ft^3/min.

Figure 16 shows the predicted SPL response as a function of frequency for HILF2 operated in this modified single-volume mode to take advantage of the lower system resonant frequency. For these calculations, the long tubular internal port was replaced by a 2-ft-square hole through the partition between the input and test volumes and the vent was three 8-in.-diam., 7.5-ft tubes as just described. For this vent arrangement (now, the tuning port), the ac flow cutoff SPL calculated from equations (C-7) and (C-8) is almost 170 dB. The compressor output was again assumed to be $F_c = 2350$ ft^3/min with $P_{max} = 13$ psig with a resulting calculated ac modulator output $P_i = 4000$ Pa and $R_f = 2145$ W at 5 Hz. The upper curve assumes wall absorption only; as above, the successively lower curves assume 4-in.-long leaks with diameters of 0.5, 0.78, and 1.0 in. The fifth curve with the double hump is the 0.5-in. leak result plotted on a 2X frequency scale from 0 to 50 Hz. This curve shows that the system still has two resonances—the 2-ft^2 hole in the partition is predicted to function as a low-mass port and generate a resonance at about $f_{rhi} = 40$ Hz. The mass of this hole is surprisingly high. Even though the hole is only 3/4 in. long (plywood thickness), end effects give it an effective length of 21 in. (see appendix A, eq A-2). Its ac cutoff SPL is over 174 dB! Even though the modulator will not operate at this high frequency, this resonance might be excited by harmonics of the modulator output.

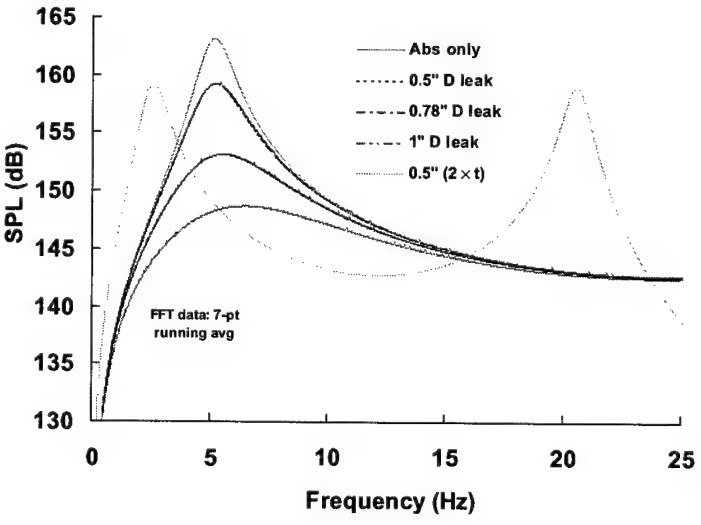

Figure 16. Calculated test volume SPL frequency response in HILF2 operated in single-volume mode with a 24- by 24-in. hole in the internal partition and three 8-in. by 7.5-ft vents as a tuning port and assuming different levels of acoustic loss (see text).

If we assume that the system losses at 5 Hz are fairly represented by a 0.78-in.-diam. leak, then, as shown in figure 15, the predicted SPL at f_{rlo} = 5.5 Hz is 153 dB. The system Q at f_{rlo} in this case is just 1.4. At this low frequency, the 0.78-in. leak imposes a severe loss on the system since the leak rate is determined almost completely by the low-velocity air viscosity alone.

Table 1 summarizes our modulator and circuit model predictions for the performance of HILF2 with the use of the nominal F_c = 2350 ft^3/min, P_{max} = 13 psig output from the air compressors.

Table 1. Summary of predicted HILF2 performance from flow modulator and circuit model results, assuming air compressor outputs, F_c = 2350 ft^3/min and P_{max} = 13 psi.

Internal port: two 10-in.-diam., 54-long ducts through partition
Vent: two 8-in.-diam., 240-in. ducts
Calculated Modulator operation at 12 Hz: P_i = 2770 Pa, R_f = 2472 Ω

Assumed loss sources	Operating resonance frequency (Hz)	SPL at peak (dB)	Net parallel loss resistance (Ω)	Q at operating resonance
Wall absorption only	13.3	159.5	9830	4.6
Wall +0.5 in.-diam., 4-in. long leak	13.3	158	4660	4.0
Wall + 0.78-in.-diam., 4-in. long leak	13.1	155.5	1915	3.0
Wall + 1.0-in.-diam., 4-in.-long leak	12.5	153	1044	2.1

Internal Port: one 24-in.-square, 3/4-in.-long hole in partition
Vent (tuning port): three 8-in.-diam., 90-in.-long ducts
Calculated modulator operation at 5 Hz: P_f = 4000 Pa, R_f = 4645 Ω

Assumed loss sources	Operating resonance frequency (Hz)	SPL at peak (dB)	Net parallel loss resistance (Ω)	Q operating resonance
Wall absorption only	5.1	163	12980	3.7
Wall + 0.5-in.-diam., 4-in.-long leak	5.2	159	4190	2.5
Wall + 0.78-in.-diam., 4-in.-long leak	5.5	153	1418	1.4
Wall + 1.0-in.-diam., 4-in.-long leak	6.4	149	727	1.0

5. Measuring the Performance of the HILF2 System

We conducted a series of performance tests on the complete two-chamber HILF system in April to June 2000. Over this period, the system was operated in a variety of configurations with various combinations of ports, vents, and compressor pulley ratios, and a number of system modifications were made in an attempt to correct problems or deficiencies that were encountered.

Early in this test series, we identified a major deficiency. As noted in section 3, in tests in which we used both 3.5-in. and 2.25-in.-diam. pulleys on the Paxton compressors with the 8-in.-diam. engine crankshaft pulley, we observed belt slippage at engine speeds corresponding to about 34,000 compressor impeller rpm—well below the specified capacity of the compressors and the horsepower rating of the engine. In an attempt to increase belt contact area with the compressor pulleys while maintaining the 1:13 engine-to-impeller rpm ratio achieved with the 2.25-in. compressor pulleys, we replaced the 8-in. crankshaft pulleys with custom 12-in.-diam. units and reinstalled the 3.5-in. compressor pulleys. We also constructed and installed a fixed idler arrangement and additional bracing of the compressor mounts to increase the serpentine belt tension. Unfortunately, these measures did not solve the problem, and we continued to observe belt slippage at about 34,000 impeller rpm. Further investigation indicated that the slippage problem is associated with just one of the compressors. The L (left side) compressor was invariably the source of the belt slippage squeal. In addition, this unit and its cooling oil output became much hotter during operation than the R (right side) unit. By contrast, we were able to run the R unit at over 47,000 rpm with the L unit disconnected. We hypothesize that the bearings or internal gear train in the L unit may be damaged and generating excess drag at high rpms. Since we lacked both time and money to seek repair of the L unit, we were forced to restrict our tests to engine and compressor speeds well below their specified capacities.

Rather than present the details and results of the many varied tests performed, we discuss here the results of tests representative of the performance of the system in its "final" form, subject to the air source operational limitations just noted.

5.1 Instrumentation for the Performance Tests

The air pressure and airflow sensors were described in section 3. For the tests described here, we recorded the time dependencies of the air pressure in the modulator surge tank and the airflow in one of the 8-in.-diam. vent ducts from the chamber input volume.

The Chevrolet engine control system included an analog tachometer and an electrical signal output from the ignition system. We determined that the analog tachometer had an accuracy of roughly ±10 percent of the indicated engine rpm. The pulses from the ignition system were processed by a frequency-to-voltage converter or could be directly counted to generate accurate measures of engine (and, thus, compressor) rpm.

We made SPL measurements in the chamber using Bruel & Kjaer capacitor microphones, model 2669 preamplifiers, and a model 5935 power supply. A model 4191 1/2-in. microphone was used in the input volume and a model 4136 microphone was used in the test volume; at a polarization voltage of 28 V, the sensitivities of these microphones were 541.1 and 6105 Pa/V, respectively.

The air pressure, flow, engine rpm, and SPL data were recorded in parallel with the use of a Tektronix TDS684A digital oscilloscope and an IOTech WaveBook 8-channel, 12-bit waveform digitizer coupled to a laptop computer.

5.2 Experimental Procedures for the Performance Tests

The dynamic speed controller for the flow modulator dc drive motor has three modes of operation: (1) set for constant rpm, (2) rpm internally programmed for sweep from a starting to an ending value, and (3) rpm externally programmed by a 0- to 10-V input voltage. Generally, we performed two types of measurements on the system: (1) single frequency, and (2) frequency sweep. To perform a single-frequency measurement, we would first set the flow modulator controller for the desired rpm (one-half the desired frequency), then start the engine and set the desired compressor rpm, and, finally, trigger the digital oscilloscope and waveform digitizer to record the SPLs and other system variables. For these single-frequency measurements, we used short recording times at moderate data-sampling rates (e.g., 4.1 s at 2 kHz for the digitizer) to provide reasonable waveform and harmonic resolution. To perform a frequency sweep, the flow modulator controller was externally driven by an analog ramp generator between preset minimum and maximum frequencies. After starting the engine again and setting its rpm, we then simultaneously triggered the ramp generator and the recording instruments. The modulator frequency would then ramp linearly from its preset minimum to maximum value. To provide high resolution of low frequencies, we used long-duration sweeps with low data-sampling rates. A 150-s measurement at 54.67 Hz provided a frequency resolution of 0.0067 Hz and a frequency range from 0 to 27.3 Hz for 8200 points.

5.3 Performance Test Results and Discussion

5.3.1 Two-Volume Test With Single Vent

We installed two 10-in.-diam, 54-in.-long internal ports in the HILF chamber and vented the input volume of the chamber to free air with a single 8-in.-diam., 21.8-ft-long metal duct. Figure 17 shows the system as it appeared with the single metal vent installed. The dual compressors are visible on the engine stand at the right ends of the two 4-in. white PVC airlines. The surge tank and two 10-in. internal port sections are visible on top of the chamber, as is the 24-in. concrete hatch cover. This system configuration is essentially the same as that described and modeled in section 5. The impeller-to-engine rpm ratio for this test was 8.6:1.

Representative test results are shown in figures 15 and 18 through 22. The jagged curve in figure 15 is SPL measured as a function of frequency in the chamber test volume with the engine operating at 2500 rpm (21,500 compressor impeller rpm). These curves were obtained by sweeping the modulator operating frequency from 2 to 25 Hz in 150 s. The resulting SPL data were analyzed with an FFT and scaled to produce the frequency response curve. Note that the general shape of the measured response and the location of the high-frequency resonance are in reasonable agreement with the previously generated model predictions shown in the figure. In particular, the shape of the model curve generated with the use of an assumed 1/2-in.-diam. leak is a close fit to the measurement above 10 Hz. The measured SPL falls well below the model curves; however, the model results were generated assuming the theoretical output of the compressors operating at 4000 engine rpm and 34,400 impeller rpm.

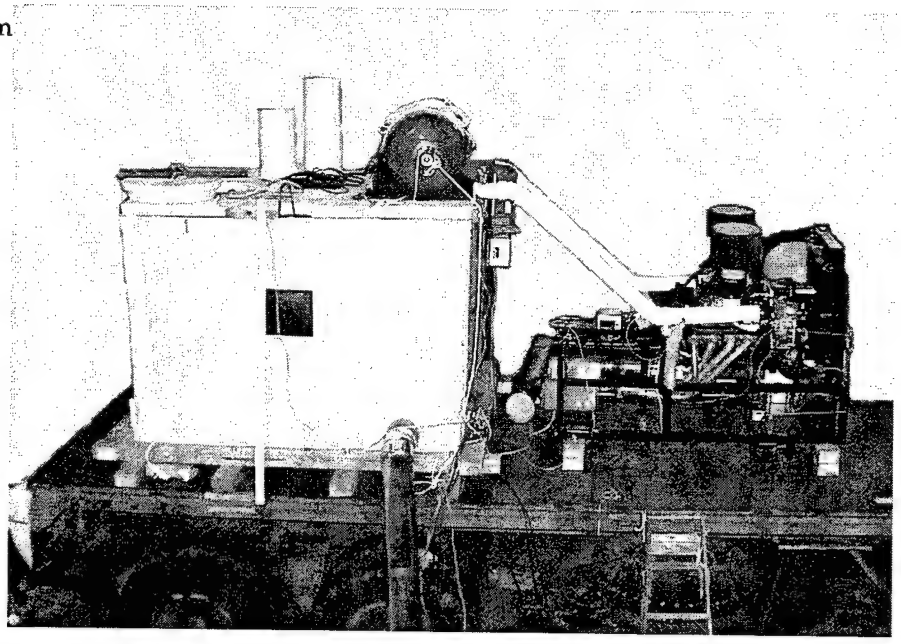

Figure 17. HILF2 system configured for initial performance tests with single 8-in. vent.

Figures 18 and 19 show instantaneous SPL waveforms recorded in the test (solid curves) and input (dashed curves) volumes at engine speeds of 2500 and 4000 rpm with the modulator operating at the nominal f_{res} = 13 Hz. Very clean sine waves were recorded in the test volumes with SPLs of 154.6 dB and 158.5 dB at 2500 and 4000 rpm. The waveforms in the input volume are distorted on the positive half-cycles by the input pressure pulse from the modulator. The SPLs in the test and input volumes are out of phase by nearly 180° as expected at resonance for the two-volume Helmholtz resonator. Figure 20 shows the acoustic spectrum of the SPL recorded in the test volume at 4000 rpm and confirms the purity of the waveform: the second harmonic is more than 25 dB below the fundamental, and the higher order harmonics rapidly fall below the noise floor. Over 99 percent of the acoustic energy is concentrated in the fundamental at 13 Hz.

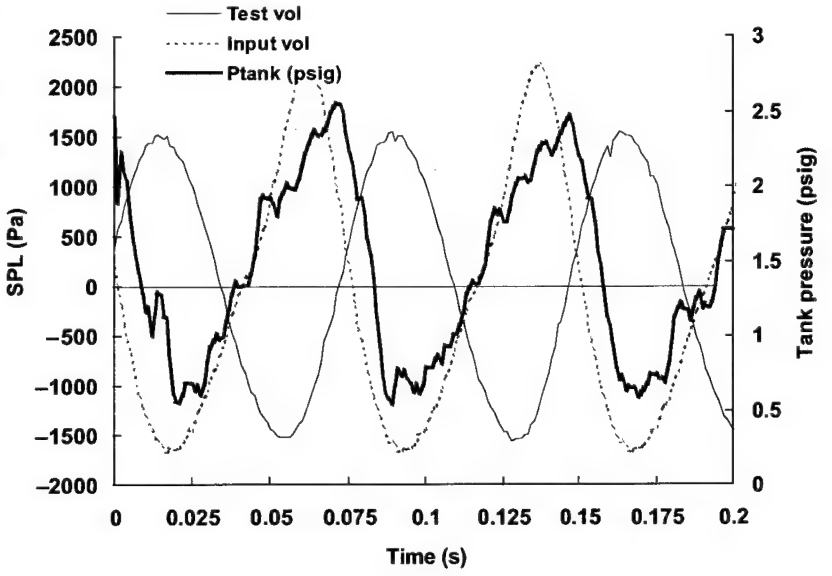

Figure 18. Test volume (solid curve), input volume (dashed curve) SPL, and surge tank pressure (gray curve) as a function of time for HILF2 operating at 13 Hz in two-volume, single-vent mode with compressor speed of 21,500 rpm.

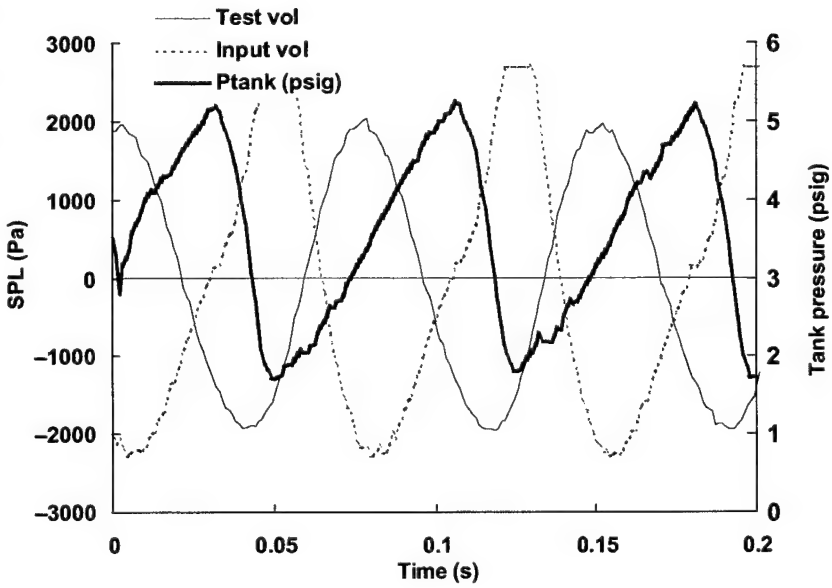

Figure 19. Test volume (solid curve), input volume (dashed curve) SPL, and surge tank pressure (gray curve) as a function of time for HILF2 operating at 13 Hz in two-volume, single-vent mode with compressor speed of 34,400 rpm.

Figure 20. Acoustic spectrum of SPL in test chamber for HILF2 operating at 13 Hz in two-volume, single-vent mode with compressor speed of 34,400 rpm.

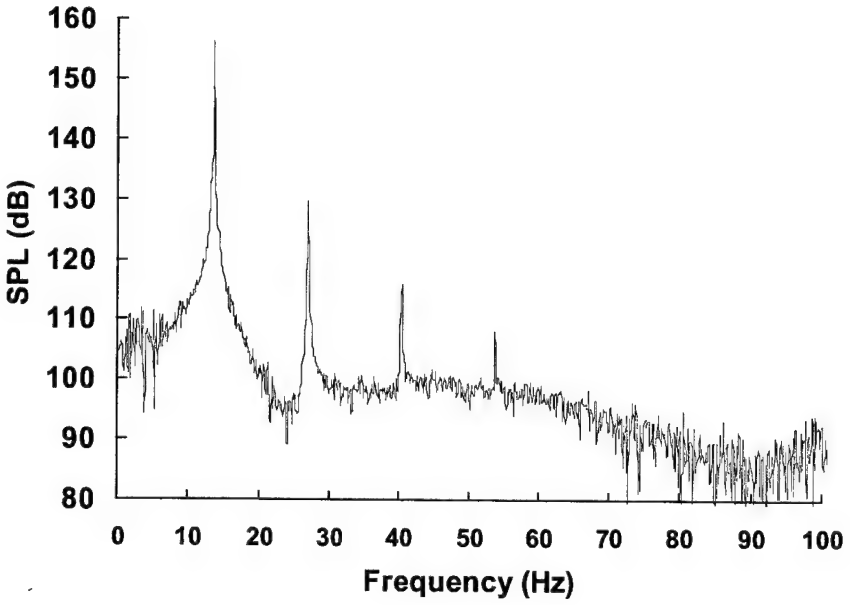

Figure 21. Measured (solid curve) and calculated (dashed curve) surge tank pressure as a function of time for HILF2 operating at 13 Hz in two-volume, single-vent mode with compressor speed of 21,500 rpm.

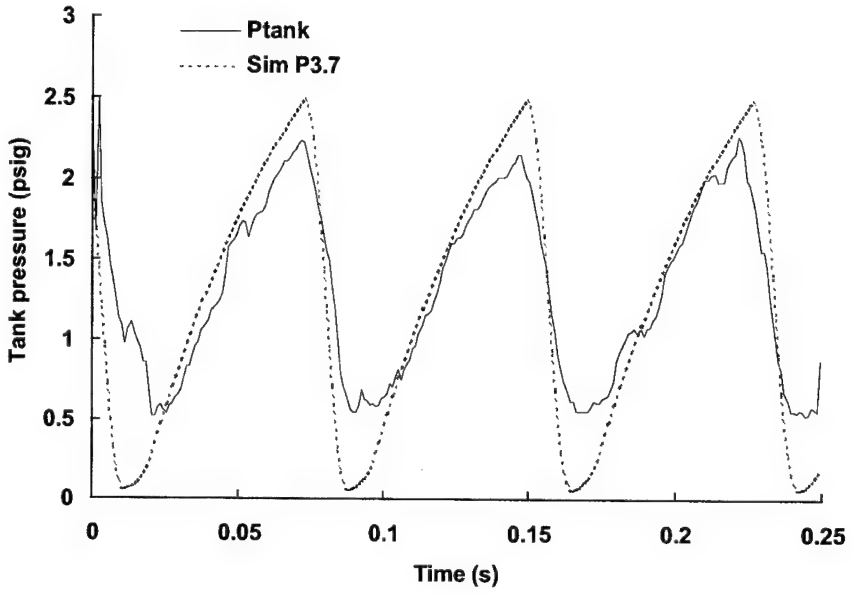

Figures 21 and 22 show the recorded (solid curve) and predicted (dashed curve) pressure in the modulator surge tank as a function of time for the modulator operating at 13 Hz with engine speeds of 2500 and 4000 rpm (8.6:1 pulley ratio). The model curves were computed as described in section 4.2, assuming P_{max} = 3.7 or 9.5 psig and F_c = 1720 or 2750 ft^3/min at 2500 and 4000 engine rpm, respectively. The observed peak tank pressures are close to the predictions in both cases, but the minimum observed pressures were much higher than expected. At 4000 rpm, we expected the tank to blow down to less than 0.4 psig at the end of each modulator ON cycle, but the minimum observed pressure was about 1.7 psig. This implied substantial backpressure in the test chamber; that is, the average (dc) test cham-

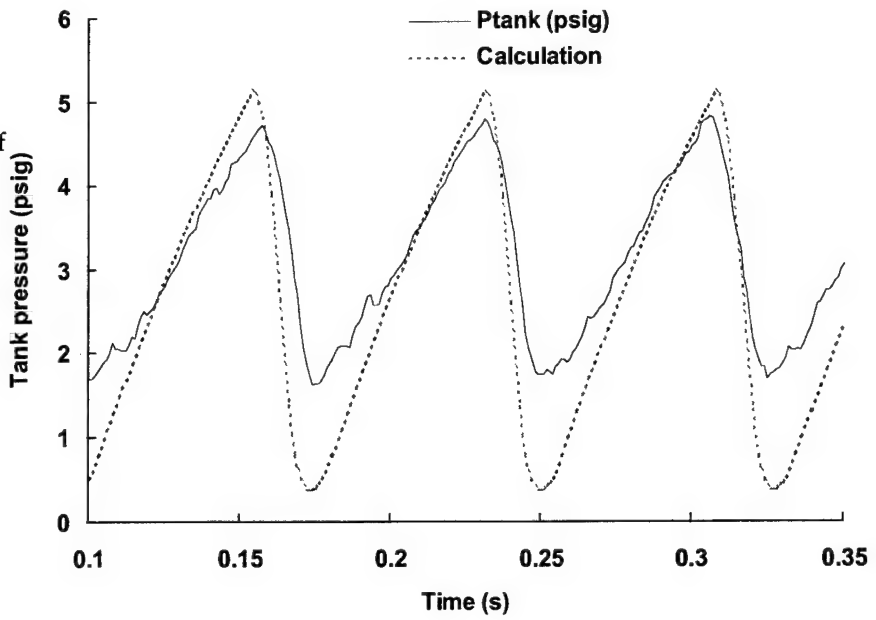

Figure 22. Measured (solid curve) and calculated (dashed curve) surge tank pressure as a function of time for HILF2 operating at 13 Hz in two-volume, single-vent mode with compressor speed of 34,400 rpm.

ber pressure was not close to ambient atmospheric pressure as we intended. In fact, following the tests we observed that the 24-in. concrete hatch on the test volume had been lifted out of position against its own weight and also against the restraint of a heavy nylon strap under high tension. In addition to applying unintended and unnecessary stress to the chamber (and on a possible test subject's eardrums), the dc backpressure reduced the pressure excursion (maximum to minimum pressure) generated by the modulator pulses and therefore the amplitude of the acoustic signal in the chamber. Evidently, the single 8-in.-diam. vent was inadequate to handle the dc airflow from the chamber without an unacceptably large pressure drop. At this point we suspended the tests pending installation of additional vents and upgraded compressor drive hardware intended to permit compressor operation at the full rated 50,000 impeller rpm.

5.3.2 Two-Volume Test With Triple Vent

For these tests, we installed two additional 8-in. ID ports with metal ducts to the input chamber. The dc airflow vent now consisted of three 8-in.-diam., 26.5-ft-long pipes in parallel. As in 5.3.1, the internal port connecting the input and test volumes consisted of two 10-in.-diam., 54-in.-long ducts.

We also installed the new 1:13.07 ratio compressor drive hardware and associated compressor mount improvements intended to permit operation at the full rated 50,000 impeller rpm. As noted above, however, belt slippage continued to limit operation of the system to an impeller speed of about 34,000 rpm at about 2500 engine rpm.

Figure 23 shows SPL (solid ragged curve) measured in the chamber test volume as a function of frequency for this system configuration with the modulator frequency swept from 2 to 25 Hz and with the compressors op-

erating at 1930 engine/rpm and 25,230 impeller rpm. The upper resonance has an SPL of about 154 dB at 12.5 Hz. Also shown in the figure (smooth curves) is the calculated response, assuming various levels of acoustic loss. The upper curve assumes wall absorption only; the successively lower curves also include increasing losses through a decreasing parallel loss resistance, R_{loss}. The observed f_{res} is slightly lower than the predicted 13 Hz; the observed Q of the system at 12.5 Hz is 2.6. The resonance peak amplitude is close to that predicted by a sum of wall absorption and other losses equivalent to $R_{loss} = 5\ k\Omega$. Figure 24 shows the waveforms recorded in the test and input volumes with the modulator operating at 13 Hz and the compressors operating at 2415 engine/31,560 impeller rpm. The test chamber SPL was 1240 Pa (155.9 dB). Note again the clean waveform in the test volume and the higher positive peak in the input volume caused by the modulator airflow pulse. Unfortunately, the compressor drive problems discussed above limited operation to below 2500 engine rpm instead of the hoped-for 4000 rpm full power level.

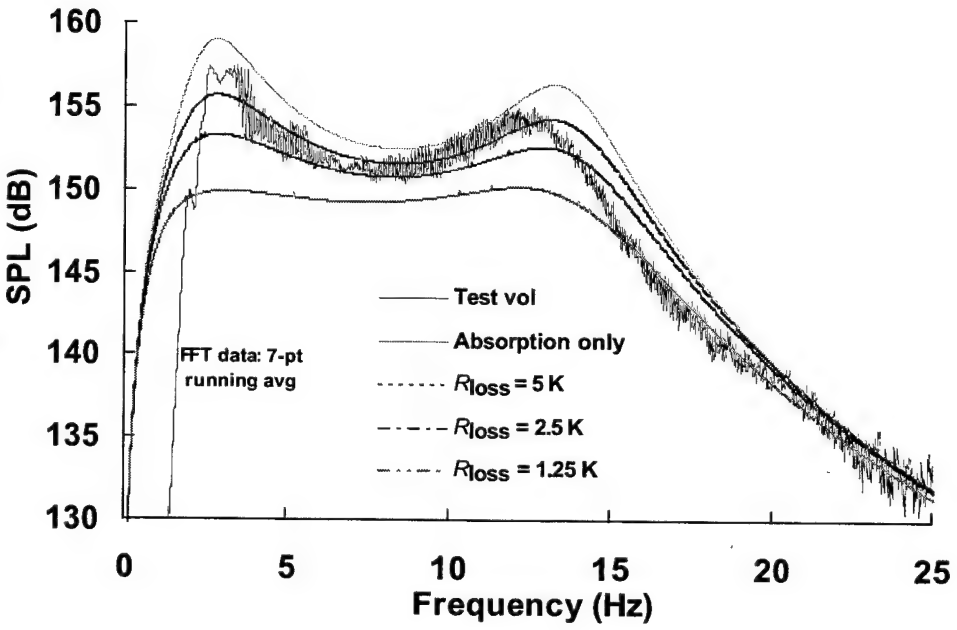

Figure 23. Measured (solid ragged curve) and calculated (smooth curves) test volume SPL frequency response in HILF2 with compressor speed of 25,230 rpm with the use of two 10-in. by 54-in. internal ports and three 8-in. by 26.5-ft vents. Calculated responses assume different levels of acoustic loss (see text).

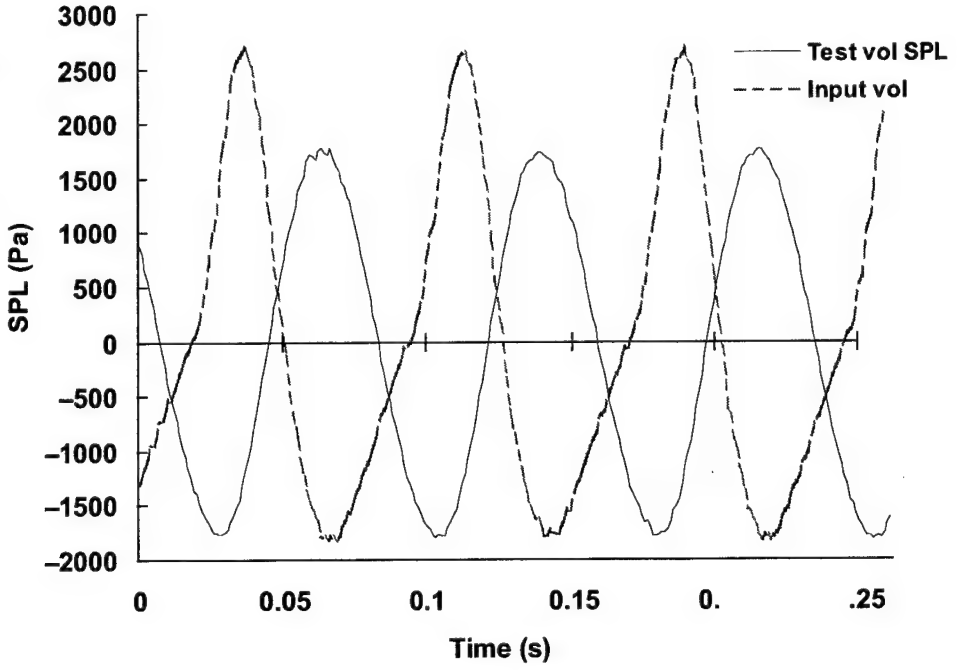

Figure 24. Test volume (solid curve) and input volume (dashed curve) SPL as a function of time for HILF2 operating at 13 Hz in two-volume, three-vent mode (see fig. 23) with compressor speed of 25,230 rpm.

5.3.4 Single-Volume Test With Triple Vent as Tuning Port

Of particular interest in figure 23 is the size of the *lower* resonant peak near 2.6 Hz. As discussed in section 5, this peak results from the response of the Helmholtz resonator formed by the compliance of the total volume of the chamber and the acoustic mass of the three 8-in.vents—the internal port has little effect on this resonance and serves merely to connect the two chamber volumes. Even though the system was not optimized to respond in this mode and at this frequency, both the model and the measurements indicated that this peak was greater in amplitude than the high-frequency resonance (about 157 dB under these operating conditions at 1930 engine rpm). Figure 25 shows the test chamber waveform and surge tank pressure recorded with the modulator operating at 2.6 Hz and with the compressors operating at 2490 engine rpm and 32,540 impeller rpm. For this case, the SPL in the test volume at 2.6 Hz was 2350 Pa (161.4 dB)! The waveform is not as pure a sinusoid as shown in figures 19 or 21. The secondary peak on the positive side of the waveform occurs at the same time as the rapid decrease in surge tank pressure associated with the airflow pulse from the modulator. The acoustic spectrum corresponding to the SPL in figure 25 is shown in figure 26. The harmonic content of the waveform is much greater than for the two-volume resonance at 13 Hz (figs. 20 and 24). Since the input and test volumes act as one in the low-frequency, single-volume resonance mode, the waveform in the test volume is not "filtered" with respect to the input volume waveform as is the case in the two-volume resonance mode. Despite this, over 90 percent of the acoustic energy in the test volume SPL is concentrated at the 2.6-Hz fundamental.

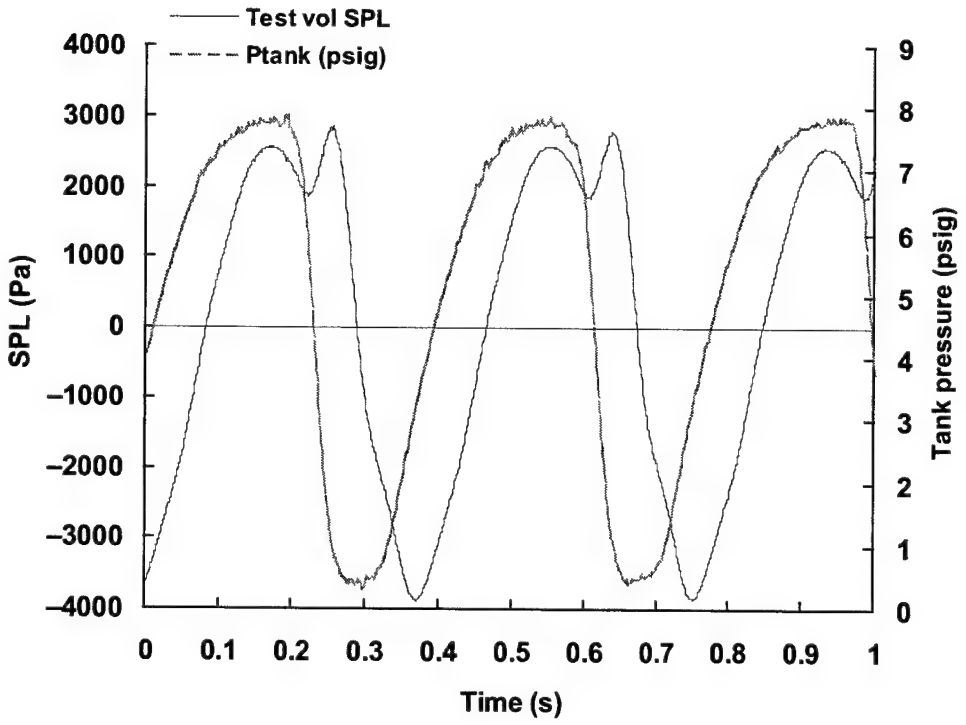

Figure 25. Test volume SPL (solid curve) and surge tank pressure (gray curve) as a function of time for HILF2 operating in single-volume mode at 2.6 Hz with the use of two 10-in. by 54-in. internal ports and three 8-in. by 26.5-ft vents with compressor speed of 32,540 rpm.

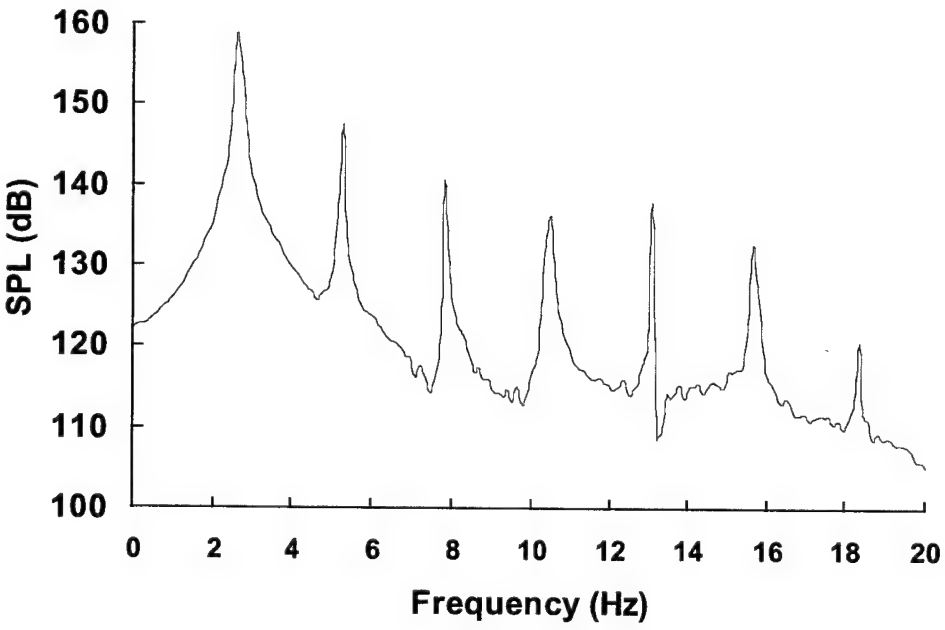

Figure 26. Acoustic spectrum of SPL in test chamber for HILF2 operating at 2.6 Hz in single-volume mode (see fig. 25) with compressor speed of 32,540 rpm.

To investigate further the response of the system in this single-volume resonance mode, we then removed the two 10-in.-diam., 54-in.-long internal ports and one plywood mounting board, leaving one 10-in. round hole and one 14- × 14-in. square hole through the partition between the input and test volumes. Effectively, we drastically reduced the acoustic mass of the internal port, raising the expected two-chamber high-frequency resonance from 13 Hz to above 40 Hz. Figure 27 shows SPL (ragged solid curve) measured as a function of frequency for a sweep from 2 to 5 Hz with the compressors operating at 2002 rpm engine rpm and 26,170 impeller rpm. The SPL at resonance (about 160 dB) is essentially unchanged from that measured near the same rpm with the 10-in. internal ports in place. Also shown in the figure are calculated responses for the system with the holes in the partition, assuming various levels of acoustic loss. Based on the shape of the measured resonance curve at and above resonance, the system Q is about 2.0. On the upper side, the measured response is reasonably well matched by the calculation that assumes only wall-absorption losses. Below resonance, the system response drops off more rapidly than predicted by the calculations. The calculations assume a constant modulator input efficiency as a function of frequency; in reality, we expect the efficiency to fall off rapidly with frequency as the modulator flow pulse duration becomes very short compared with the modulator's operating period.

Finally, figure 28 shows the measured and calculated frequency response of the system with the three vents reduced in length to 11.75 ft and with the compressors operating at 1930 engine rpm and 25,200 impeller rpm. The reduced vent mass raised the measured single-volume resonance peak to about 4.4 Hz; the intensity at resonance at this rpm was about 159 dB and the system Q was about 2.0.

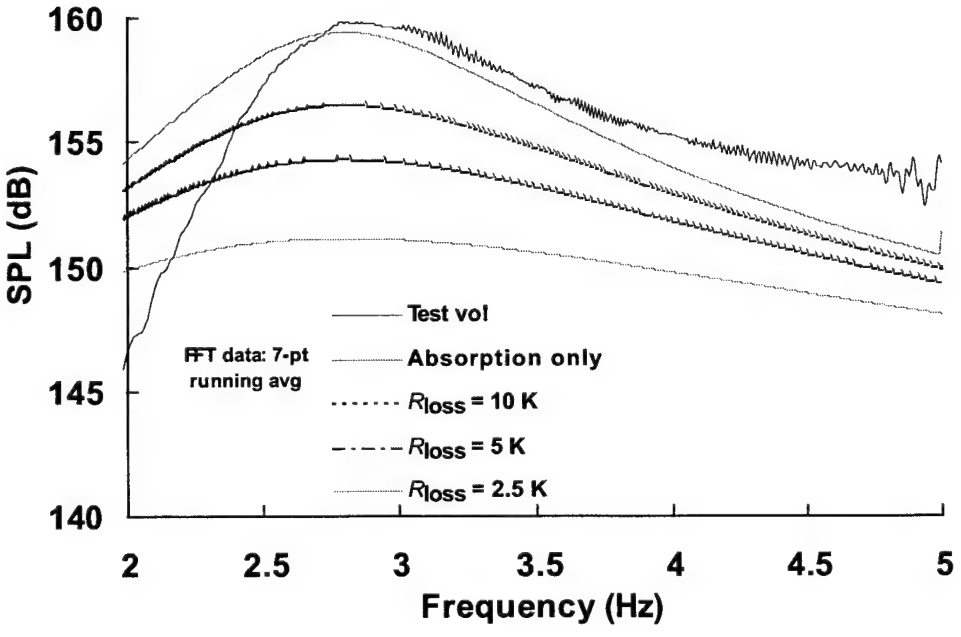

Figure 27. Measured (solid ragged curve) and calculated (smooth curves) test volume SPL frequency response in HILF2 with compressor speed of 26,170 rpm with two holes in internal partition and three 8-in. by 26.5-ft vents. Calculated responses assume different levels of acoustic loss (see text).

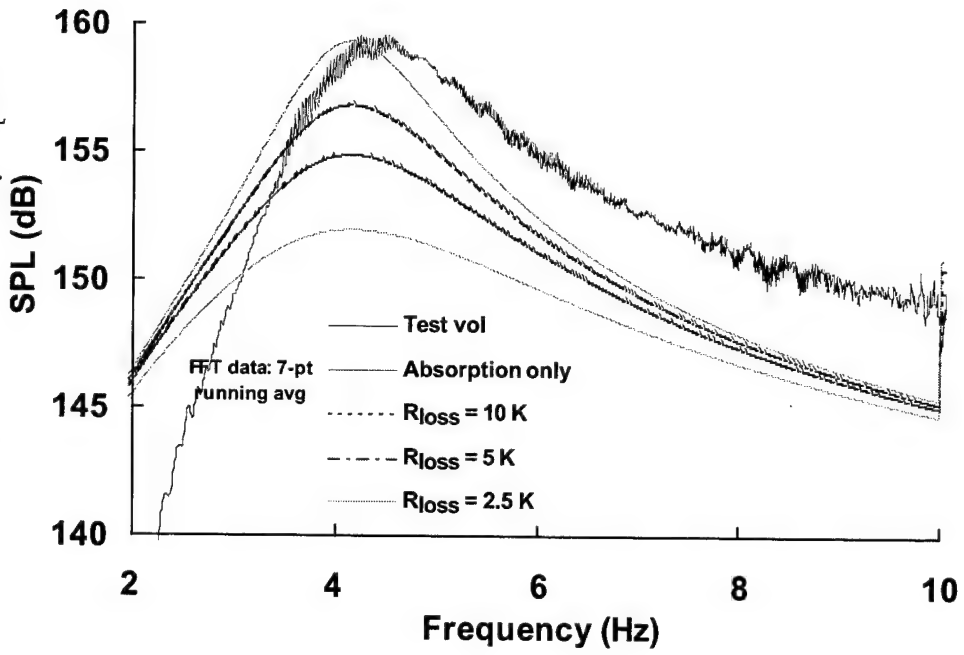

Figure 28. Measured (solid ragged curve) and calculated (smooth curves) test volume SPL frequency response in HILF2 with compressor speed of 25,200 rpm with two holes in internal partition and three 8-in. by 11.75-ft vents. Calculated responses assume different levels of acoustic loss (see text).

5.3.5 Summary of Test Results

Table 2 summarizes the performance test results just presented. In general, the measured performance of the HILF2 system is in reasonable agreement with the predicted performance from our model calculations. Comparing table 2 with the calculated response in table 1 for the system operating with compressor outputs of F_c = 2350 ft^3/min and P_i = 13 psig, at 13 Hz with the two-volume single-vent configuration, we achieved an SPL corresponding approximately to the predicted performance, assuming losses only slightly greater than wall absorption alone. Taking into account the substantially lower airflow power available with the compressor operating at 25,200 rather than 35,000 rpm, the system performance at 4.4 Hz is similarly in line with the predictions for 5 Hz. We achieved our target maximum SPL in excess of 160 dB (2000 Pa) at 2.6 Hz, even though the compressor rpm was limited to 35,000 rpm rather than the design maximum of 50,000 rpm. Given the cubic dependence of airflow power on compressor rpm, we therefore achieved our goal with one-third the expected power input.

Table 2. Partial summary of HILF2 measured performance.

Configuration	Engine rpm	Impeller rpm	F_c (cfm)	P_{max} (psig)	f (Hz)	SPL (Pa)	SPL (dB)
2 vol, two 20- × 54-in. internal ports, one 8-in. × 21.8-ft. vent	2507	21,560	1720	3.7	13.0	1070	154.6
	4035	34,700	2750	9.5	13.0	1680	158.5
2 vol, two 20- × 54-in. internal ports, three 8-in. × 26.5-ft. vents	1930	25,230	2020	5.1	12.5	1000	154.0
	2415	31,560	2525	8.0	13.0	1240	155.9
1 vol, three 8-in. × 26.5-ft. vents/port	2490	32,540	2600	8.5	2.6	2350	161.4

6. Recommendations for Further Work

While we were successful in meeting the performance goals for the infrasonic test system, we could not claim as of the time of this report that we had produced "a reasonably portable and reliable system capable of being moved to a research facility and used in long-term acoustic effects experiments" (sec. 4, task 4). During the performance tests, several deficiencies and some outright failures of system components became evident in HILF2. In addition, HILF2 as configured for the performance tests was not very suitable or user-friendly for its ultimate purpose—supporting high-intensity acoustic effects experiments—and it was not really portable, that is, capable of being moved (road worthy) and used at sites other than ARL. Further work on the HILF system could range from making essential repairs and modifications on the existing system to obtain a working test system at minimum cost to performing a major reconstruction of the system to enhance its performance and versatility and streamline its use by second-party experimentalists (turnkey system). We outline some specific tasks in appendix D.

7. Conclusions

We have designed, modeled, and tested an improved high-intensity infrasonic test system—HILF2. This unique system includes a dedicated high-capacity compressed-air source, a low-impedance airflow modulator of our own design, and a novel two-volume Helmholtz resonator/test chamber. The system design was aided and confirmed through the use of a series of *ad hoc* computer-based computational models of the air source, modulator, and resonator subsystems. System performance tests demonstrated that we were successful in achieving the goal of generating in the 2.4-m^3 test volume sustained, high-spectral-purity SPLs in excess of 155 dB at frequencies from 2.6 to 13 Hz. At full available power from the air source, levels of 161.4 and 158.5 dB were achieved at 2.6 and 13 Hz, respectively. We believe that this performance is unequalled. With some additional effort to correct identified deficiencies, the HILF system can provide a unique large-volume, spectrally clean, controllable acoustic environment for materiel, biological, and human effects experiments at frequencies and intensities only marginally available at other facilities.

8. Acknowledgments

The authors wish to thank Bill Davis and Brent Warren of the ARL Blossom Point Research Facility for their support of the early field experiments and for transport of the chamber. We also thank John Noble and Mark Coleman of ARL for their interest and participation in the early experiments with the ARL Mobile Acoustic Source and we express thanks to Charlie Brown of ARL for his aid and support at several stages of the effort. Finally, we particularly acknowledge Harry Moore of ARDEC for his continuing interest in and support of this work.

9. References

1. Boesch, H. E., Jr., B. T. Benwell, and C. G. Reiff, *Design and Test of a Prototype Acoustic High-Intensity Infrasonic Test Chamber*, ARL-TR-2137 (April 2000).
2. Beranek, L. L., *Acoustics*, McGraw-Hill, New York (1954).
3. Seto, W. *Theory and Problems of Acoustics* (1971).
4. Sabatier, J. M., *Pneumatic Loudspeaker Acoustic Generator System*, Technical Report, National Center for Physical Acoustics, University of Mississippi (1991).

Appendix A. Lumped-Parameter Acoustic Elements

The acoustic elements we used for modeling the response of the HILF system include the source elements, the loss elements, and the reactive elements.

The acoustic energy source (flow modulator) is represented as a time-varying single-frequency (sinusoidal) RMS input pressure, P_{in} (equivalent to an ac electrical voltage source) in series with a characteristic resistance, R_f. In our case, the actual source is a complex system consisting of the air compressors, surge tank, and flow modulator. We describe the derivation of P_{in} and R_f from the characteristics of this system in section 4.

The reactive elements are acoustic compliances associated with air compressibility in volumes and acoustic masses associated with the inertia of air (usually in tubes) moving under acoustic excitation. The compliances, C_{ac}, in m^3 per Pa associated with the chamber volumes are given by

$$C_{ac} = V / (\gamma P_0) \ , \qquad \text{(A-1)}$$

where V is the volume in m^3, γ is the ratio of the specific heats for air, and P_0 is the ambient atmospheric pressure. The masses, M_a, in kg per m^4 of the port and vent are given by

$$M_a = \rho_0 [L + k\,a]/(A\,n) \qquad \text{(A-2)}$$

where ρ_0 is the density of air, L is the length of the tube associated with the port or vent, a is its effective radius, and A is its cross-section area. If multiple identical ports are used in place of a single larger port, n is the number of ports.

The quantity in square brackets in eq. (A-2) is the *effective* length of the port: k is a constant associated with the additional mass contributed by tube end effects; for example, each end of a tube that is flush with a large surface contributes 0.85 to k. Free ends each contribute 0.613 to k.

Loss elements include acoustic absorption by the walls of the chamber, R_{wall}, viscous losses in the port, R_{ap}, and radiation of acoustic energy to the external environment (radiation resistance), R_{ar}:

$$R_{wall} = 2\,g\,P_0/(c\,k_{abs}\,S) \ , \qquad \text{(A-3)}$$

where c is the speed of sound, k_{abs} is the frequency-dependent acoustic absorption coefficient for the wall material [1] and S is the wall area exposed to the sound. Note that this expression applies when R_{wall} is treated as a leakage of energy to the outside (ground), that is, is in *parallel* with the chamber compliances. Thus, larger values of R_{wall} correspond to smaller losses.

The kinetic acoustic resistance of a tube or duct is

$$R_{ak} = \rho_0 [L/a + 2] (4 \pi \mu f)^{1/2}/(A n) , \quad \text{(A-4)}$$

where μ is the kinetic viscosity coefficient for air (1.56×10^{-5} m^2/s at standard temperature and pressure (STP)) and f is the frequency in Hz.

At audible frequencies, acoustic resistances are generally modeled with the use of only the kinetic viscosity of air (eq (A-5)); however, since R_{ak} decreases with decreasing frequency, at very low frequencies, R_{ak} becomes small and the flow resistance, R_{as}, associated with the static or low velocity viscosity of the air becomes significant:

$$R_{as} = 8 \pi \eta L/(A^2 n) , \quad \text{(A-5)}$$

where h is the low-velocity viscosity of air. To effect a smooth transition between R_{ak} and R_{as}, we treated them as one term, R_a, after adding them as the square root of the sum of their squares:

$$R_a = (R_{as}^2 + R_{ak}^2)^{1/2}. \quad \text{(A-6)}$$

An additional source of acoustic loss is the frequency-dependent radiation of acoustic energy from ports or vents connected to the outside. This is characterized by the radiation resistance, R_{ar}:

$$R_{ar} = \pi f^2 n^2 \rho_0 / c , \quad \text{(A-7)}$$

Note that R_a and R_{ar} are resistances in *series* with the ports or vents (larger values correspond to larger losses).

Appendix B. Calculation of Modulator Flow as a Function of Pressure

The derivation of the expressions for volume airflow, F_m, through the flow modulator follows the treatment given in [4]. The basic expressions for compressible flow are:

$$P_0/P = [1 + (\gamma - 1)M^2/2]^{\gamma/(\gamma-1)}, \quad \text{(B-1)}$$

$$T_0/T = [1 + (\gamma - 1)M^2/2], \quad \text{(B-2)}$$

and

$$\rho_0/\rho = [1 + (\gamma - 1)M^2 / 2]^{1/(\gamma-1)}, \quad \text{(B-3)}$$

where P, T, and r are the variables, T_0 and P_0 are 273 K and 1 standard atmosphere, respectively, r_0 is the density of air at STP, and γ is the ratio of specific heats for air. The mass flow rate, m_a, through the modulator aperture of area A_m is:

$$m_a = r_0 (r/r_0) c_m M A_m, \quad \text{(B-4)}$$

where M is the flow Mach number and c_m is the static speed of sound at the modulator input. We have

$$c = [\gamma R T]^{1/2}, \quad \text{(B-5)}$$

where R is the ideal gas constant. From equation (B-1), we obtain

$$M = \{(2/(\gamma-1) [10^{((\gamma-1)/\gamma) \log (Pin/Patm)} - 1]\}^{1/2}, \quad \text{(B-6)}$$

where P_{in} is the input pressure to the aperture and P_{atm} is the ambient pressure. In turn, from equations (B-2) and (B-5) we obtain

$$c_m = [\gamma R T_{in} /(1 - (\gamma - 1)M^2/2)]^{1/2}. \quad \text{(B-7)}$$

From the ideal gas law, we also obtain

$$\rho_{in} = P_{in}/(R T_{in}). \quad \text{(B-8)}$$

We then substitute equations (B-1), (B-7), and (B-8) into (B-4) to obtain

$$m_a = P_{in} \gamma^{1/2} (R T_{in})^{-1/2} [1 - (\gamma - 1) M^2/2]^{-[(\gamma+1)/2(\gamma-1)]} M A_m. \quad \text{(B-9)}$$

The modulator volume flow, F_m, is simply m_a/ρ_{atm}, where

$$\rho_{atm} = \rho_0 [P_{atm} T_0/P_0 T_{atm}], \quad \text{(B-10)}$$

and T_{atm} is the ambient air temperature. In the BASIC flow modulator calculations, we first obtain the Mach number, M, for the flow through the aperture using equation (B-6) and the input conditions. (For calculated $M >= 1$, the actual flow is saturated or choked on the input side at Mach 1 and we restrict M to be less than or equal to 1.) ρ_{atm} is calculated with the use of equation (B-10) and finally F_m is calculated with the use of equation (B-9).

Appendix C. Acoustic Mass and Energy Loss in Ports or Vents

We consider two sources of loss of acoustic mass and energy in a duct or tube used as a port or vent. The first is associated with a continuous flow of air through the duct such as may be caused by the dc airflow component from a flow modulator. For a Helmholtz resonator, at some point during an acoustic cycle at the frequency, f_{res}, the duct contains *all* of the acoustic energy in the system in the form of kinetic energy of the air in the duct. If this air is exhausted from the system, that acoustic energy is lost. To approximate the effect of an energy loss of this kind on the system, we assume that the energy loss is proportional to one-half of the volume of air in the duct that is removed per cycle. Since $1/Q$ is the fraction of energy lost to the system during each cycle, we can write

$$1/Q = (1 - 1/Q_0)(1/Q_f) + 1/Q_0 , \qquad \text{(C-1)}$$

where Q_0 is the initial system Q and Q is the net system Q with the dc flow losses included. The first term is the fractional energy loss per cycle from the dc flow; the second term is the initial energy loss per cycle. This leads to

$$Q = Q_0 Q_f/(Q_0 + Q_f - 1) . \qquad \text{(C-2)}$$

If we assume that roughly one-half of the energy in the system is lost when the dc airflow in the port per cycle equals the volume of the port, we have

$$1/Q_f = 1/2[V_{dc}/(V_p f)] , \qquad \text{(C-3)}$$

where V_{dc} is the rate of dc airflow through the port in m^3/s and f is the frequency. We now define the threshold for serious system performance loss caused by dc flow as the flow, V_{dcmax}, that results in a reduction of the system Q by a factor of two. Substituting $Q_0/2$ for Q in eq (C-1) we obtain

$$Q_f = Q_0 - 1 . \qquad \text{(C-4)}$$

Equations (C-3) and (C-4) then yield

$$V_{dcmax} = 2 V_p f/(Q_0 - 1) . \qquad \text{(C-5)}$$

As an example, consider an 8-in.-diam., 20-ft.-long port (vent), f = 13 Hz, and an initial system Q_0 = 3.0. The port volume is then 0.2 and V_{dcmax} = 2.6 m^3/s. At 2350 cfm, V_{dc} = 1.11 m^3/s—short of V_{dcmax}, but close enough to suggest that significant performance loss may occur. At 5 Hz, V_{dcmax} = 1.0 m^3/s and we are at the limit. A larger diameter port (or more of them) should be used.

The second source of loss in ports is associated with flow through the port driven by the ac component of the pressure in the chamber—the sound itself. Consider a port (duct or tube) with volume V_p attached to a larger volume (e.g., the HILF2 test volume), V_1. If V_1 is to be driven to a pressure

change, Δp, via the port, a volume ΔV_1 of air must be driven through the port into V_1. From the gas laws, we have

$$(P_0 + \Delta p)\,(V_1 + \Delta V_1)^{\gamma} = P_0\,V_1^{\gamma}\,, \tag{C-6}$$

which leads to

$$1 + \Delta V_1/V_1 = [P_0/(P_0 + \Delta p)]^{1/\gamma}\,, \tag{C-7}$$

where P_0 is atmospheric pressure. This may be rearranged to yield

$$\Delta p = \{[1 + \Delta V_1/V_1]^{-\gamma} - 1\}\,P_0\,. \tag{C-8}$$

If we assume that the port will lose its effectiveness as an acoustic mass if ΔV_1 approaches V_p, then

$$\Delta p = \{[1 + V_p/V_1]^{-\gamma} - 1\}\,P_0\,. \tag{C-9}$$

Δp now represents the "cutoff" peak (instantaneous) SPL for the system. This cutoff may be considered the acoustic equivalent of the saturation of ferromagnetic inductors by the current in the inductor. Expressed in dB, the critical SPL for the system is then

$$\text{cutoff SPL} = 20\log_{10}(|\Delta p|/(2^{1/2} * 2 \times 10^{-5}))\,. \tag{C-10}$$

To maximize the cutoff SPL, we should maximize V_p. Since we generally have a target port mass (to set the system resonant frequency, f_{res}), this argues for ports with large areas. Doubling the area (or number) of ports requires doubling the port length to maintain the same port mass; thus, the port volume is quadrupled. For the HILF2 system with $V_1 = 2.5$ m^3 (test volume), a single 10-in.-diam., 28-in.-long port results in $f_{res} = 12$ Hz and a cutoff SPL of about 157 dB. If we use two 56-in. ports to obtain the same f_{res}, the cutoff SPL is raised to 168.5 dB.

Appendix D. Possible Further Work on the HILF System

D-1. Correct Failures/Deficiencies in Present System

The following tasks should be completed to produce, at minimum cost and effort, a system that can be used for basic acoustic effects experiments at offsite (non-ARL) locations:

1. Locate and fix compressor drive problem (repair bad Paxton compressor?)
2. Replace metal vent ducts with large-diameter PVC pipe. (lightweight metal heat ducts used for vents collapsed and fractured under cyclic pressure variations produced by high SPL operation)
3. Upgrade mounting of system components (chamber, engine stand, surge tank, and modulator) on trailer and provide weather protection to allow safe road transport of system.
4. Document system operation and maintenance.

D-2. Make System More User-Friendly as an Acoustic Source

These tasks may be performed (at increasing cost and effort) to produce a system that is more versatile, has higher performance, and is more easily used for acoustic effects experiments, particularly by second-party experimenters:

1. Upgrade compressor mounts and belt drives (larger serpentine belt or timing-belt drive) to allow long-term operation at higher power levels.
2. Alter flow modulator belt drive to extend operation to lower frequencies (below 2 Hz).
3. Replace present tuning ports through internal partition in chamber with external adjustable-length large-diameter PVC duct "U-tube" connecting test and input volumes. This externally located tuning duct would allow the use of larger, longer ports to reach lower frequencies while retaining the advantages of two-volume operation and would also permit easy adjustment of system tuning without entering the chamber.
4. Replace chamber top access hatch with side door in test volume to allow easier, faster access to experimental volume.
5. Add "switchable" additional surge tank capacity to improve low-frequency (single-Hz) operation.

6. Replace existing concrete chamber (commercial grease trap) with custom-fabricated cast reinforced concrete chamber with internal concrete partition and provisions for all ports and vents, modulator mounting, and side-mounted access doors.
7. Add loudspeaker drive capability. For use at SPLs below 140 dB, a loudspeaker module that would replace the flow modulator could drive the system. This drive system would be much easier to control and would allow indoor system use for experiments not requiring the higher SPLs.
8. Upgrade all system controls to provide a "turn-key" operational capability and simplify use of the system by second-party experimenters.

Distribution

Admnstr
Defns Techl Info Ctr
ATTN DTIC-OCP
8725 John J Kingman Rd Ste 0944
FT Belvoir VA 22060-6218

TACOM/ARDEC
ATTN AMSTA-AR-CCL-D C Freund
ATTN AMSTA-AR-QAC K Yagrich
Picatinny Arsenal NJ 07806

TACOM/ARDEC
ATTN AMSTA-AR-CCL-D H Moore
Bldg 79
Picatinny Arsenal NJ 07806-5000

Directed Energy Technologies, Inc.
ATTN B Benwell
5425 Tall Cedars Rd
Sumerduck VA 22742

Pacific Northwest Natl Lab
ATTN K8-41 R Shippell
PO Box 999
Richland WA 99352

US Army Rsrch Lab
ATTN AMSRL-CI-IS-R Mail & Records Mgmt
ATTN AMSRL-CI-IS-T Techl Pub (2 copies)
ATTN AMSRL-CI-OK-TL Techl Lib (2 copies)
ATTN AMSRL-IS-EE J Noble
ATTN AMSRL-IS-EE M Coleman
ATTN AMSRL-SE-D E Scannell
ATTN AMSRL-SE-DE C Reiff (5 copies)
ATTN AMSRL-SE-DS E Boesch Jr (20 copies)
ATTN AMSRL-SE-DS J Tatum
ATTN AMSRL-SE-DP A Kehs

REPORT DOCUMENTATION PAGE

Form Approved
OMB No. 0704-0188

1. AGENCY USE ONLY *(Leave blank)*	2. REPORT DATE	3. REPORT TYPE AND DATES COVERED
	November 2001	Final, 6/99—6/00

4. TITLE AND SUBTITLE A High Intensity Infrasonic Acoustic Test System

5. FUNDING NUMBERS
DA PR: AH94
PE: 62705A

6. AUTHOR(S) H. Edwin Jr. Boesch (ARL), Christian G. Reiff (ARL), Bruce T. Benwell (Directed Energy Technologies)

7. PERFORMING ORGANIZATION NAME(S) AND ADDRESS(ES)
U.S. Army Research Laboratory
Attn: AMSRL-SE-DS email: eboesch@arl.army.mil
2800 Powder Mill Road
Adelphi, MD 20783-1197

8. PERFORMING ORGANIZATION REPORT NUMBER
ARL-TR-2349

9. SPONSORING/MONITORING AGENCY NAME(S) AND ADDRESS(ES)
TACOM/ARDEC
Picatinny Arsenal NJ 07806

10. SPONSORING/MONITORING AGENCY REPORT NUMBER

11. SUPPLEMENTARY NOTES
ARL PR: 0NE6YY
AMS code: 622705.H94

12a. DISTRIBUTION/AVAILABILITY STATEMENT Approved for public release; distribution unlimited.

12b. DISTRIBUTION CODE

13. ABSTRACT *(Maximum 200 words)*

We describe the design, mathematical modeling, construction, and test of an acoustic test system intended to support the performance of high-intensity acoustic effects experiments on large targets at low-sonic to infrasonic frequencies. An early experimental version of the system, HILF1, used a compressed-air source and airflow modulator from the ARL Mobile Acoustic Source (MOAS) and a single-volume Helmholtz resonator test chamber to achieve sound pressure levels (SPL) above 140 dB in a 5-m^3 volume. Based on results from this system, a more advanced system, HILF2, was designed and built. HILF2 uses a compressed-air source based on automotive superchargers, a low-impedance airflow modulator, and a two-volume Helmholtz resonator test chamber to achieve sustained high-purity sinusoidal sound pressure levels in excess of 155 dB in a 2.5-m^3 test volume at frequencies from 2 to 20 Hz.

14. SUBJECT TERMS	15. NUMBER OF PAGES
Helmholtz resonator, flow modulator, sound pressure, acoustic weapons	66
	16. PRICE CODE

17. SECURITY CLASSIFICATION OF REPORT	18. SECURITY CLASSIFICATION OF THIS PAGE	19. SECURITY CLASSIFICATION OF ABSTRACT	20. LIMITATION OF ABSTRACT
Unclassified	Unclassified	Unclassified	UL

NSN 7540-01-280-5500

Standard Form 298 (Rev. 2-89)
Prescribed by ANSI Std. Z39-18
298-102